

Chapter 3

Microgeometry of Composites and Their Piezoelectric Coefficients g_{ij}^*



Abstract Piezoelectric coefficients g_{ij} represent a link between an external mechanical stress applied to a sample and an electric field formed by polarisation charges of the sample as a result of the direct piezoelectric effect. The piezoelectric coefficients g_{ij} also characterise a link between a strain and electric displacement at the converse piezoelectric effect. The piezoelectric sensitivity associated with g_{ij} is of importance for sensor, energy-harvesting, acoustic, and hydroacoustic applications, for piezo-ignition systems, etc. Examples of the effective piezoelectric coefficients g_{ij}^* , $\max g_{33}^*$ and their links to the piezoelectric coefficients d_{ij}^* are discussed for piezo-active composites with various connectivity patterns (2–2-type, 1–3-type, 1–1-type, 0–3-type, and 3– β composites). The important role of the microgeometric factor and polymer component at achieving the large values of g_{ij}^* of the composite is shown.

As follows from (1.9), the piezoelectric coefficients g_{ij} represent a link between an external mechanical stress σ_j applied to a sample and an electric field E_i formed by polarisation charges of the sample as a result of the direct piezoelectric effect. In accordance with (1.8), the piezoelectric coefficients g_{ij} are used to describe the link between a strain ξ_j and electric displacement D_i at the converse piezoelectric effect [1]. The aforementioned link of the direct piezoelectric effect means that an output voltage (or electric field, or electric signal) is generated by the applied stress field (or a load). The PS associated with this generation is of importance for sensor, energy-harvesting, acoustic, and hydroacoustic applications, for piezo-ignition systems, for measuring and for quality control during production [1–6], etc. Equations (1.20) and (1.22) suggest that the piezoelectric coefficients d_{ij} studied in Chap. 2 and the piezoelectric coefficients g_{ij} to be analysed in this chapter are linked by dielectric properties that are described by a second-order rank tensor. We remind the reader that the piezoelectric properties are described by a third-rank tensor, and therefore, a link between g_{ij} and d_{ij} seems to be relatively simple due to the lower rank of the tensor of the dielectric properties.

In this chapter we discuss the PS of some modern two- and three-component composites in the context of their effective piezoelectric coefficients g_{ij}^* and relations

between d_{ij}^* and g_{ij}^* . Hereby we consider examples of the connectivity patterns, that were introduced in Chap. 2, to show the role of the microgeometric factors leading to large values of $|g_{ij}^*|$ in the composites.

3.1 2–2-Type Composites

The simplicity of the 2–2 composite structure shown in Figs. 2.1 and 2.2 and various possibilities of varying the electromechanical properties and related parameters of the piezo-active composites in wide ranges [7–11] make the 2–2 connectivity attractive to analyse its PS in the context of the piezoelectric coefficients g_{ij}^* . In Sect. 3.1 we consider examples of the PS of parallel-connected composites based on SCs poled along specific crystallographic directions.

As is known from various literature data [8, 10–13], the high-performance 2–2-type composites are often based on relaxor-ferroelectric SCs such as PMN–xPT or PZN–xPT. However these SCs are characterised by small values of the piezoelectric coefficient g_{33} in comparison to some ferroelectric materials. For example, in the [001]-poled SC from the $4mm$ symmetry class, g_{33} is linked with the piezoelectric coefficient d_{33} in accordance with (1.20) by the relation $g_{33} = d_{33}/\epsilon_{33}^\sigma$, where ϵ_{33}^σ is the dielectric permittivity of the stress-free sample. Based on experimental data from Table 1.3, we obtain for the PMN–0.33PT SC $g_{33} = 38.9$ mV/m/N. Using experimental data from Table 1.2, we obtain for the KNNTL:Mn SC $g_{33} = 94.7$ mV/m/N. Such a large g_{33} value is achieved in the SC sample where d_{33} is about 5.2 times smaller than d_{33} of the PMN–0.33PT SC, and ϵ_{33}^σ is about 12.6 times smaller than ϵ_{33}^σ of the PMN–0.33PT SC. Moreover, the KNNTL:Mn SC is a lead-free ferroelectric material that can be of interest due to its remarkable electromechanical properties.

To predict the volume-fraction behaviour of the effective properties of the 2–2-type composite, we apply the matrix method [7, 8, 11]. We show examples of the volume-fraction dependence of the piezoelectric coefficients g_{ij}^* (Fig. 3.1) in the parallel-connected 2–2-type composites. These composites are from the $mm2$ symmetry class, and relations between their piezoelectric coefficients g_{ij}^* and d_{ij}^* are represented in accordance with (1.20) as follows:

$$g_{3j}^* = d_{3j}^*/\epsilon_{33}^{*\sigma}, \quad g_{24}^* = d_{24}^*/\epsilon_{22}^{*\sigma} \quad \text{and} \quad g_{15}^* = d_{15}^*/\epsilon_{11}^{*\sigma}, \quad (3.1)$$

where $j = 1, 2$ and 3 . As for the piezoelectric coefficient d_{15}^* in the 2–2 composites analysed in Sect. 2.1 (see Figs. 2.3–2.7), the g_{15}^* is concerned with the ‘sleeping PS’ of the composite. The relatively small g_{15}^* value in a wide volume-fraction range (curve 1 in Fig. 3.1) is due to the small d_{15}^* values and the slow increase of the dielectric permittivity $\epsilon_{11}^{*\sigma}$, see (3.1). The composite structure shown in Fig. 2.2 suggests that the OX_1 direction is unfavourable to develop a high PS because there is a system of planar interfaces $x_1 = \text{const}$ in the 2–2 composite. In contrast to g_{15}^* ,

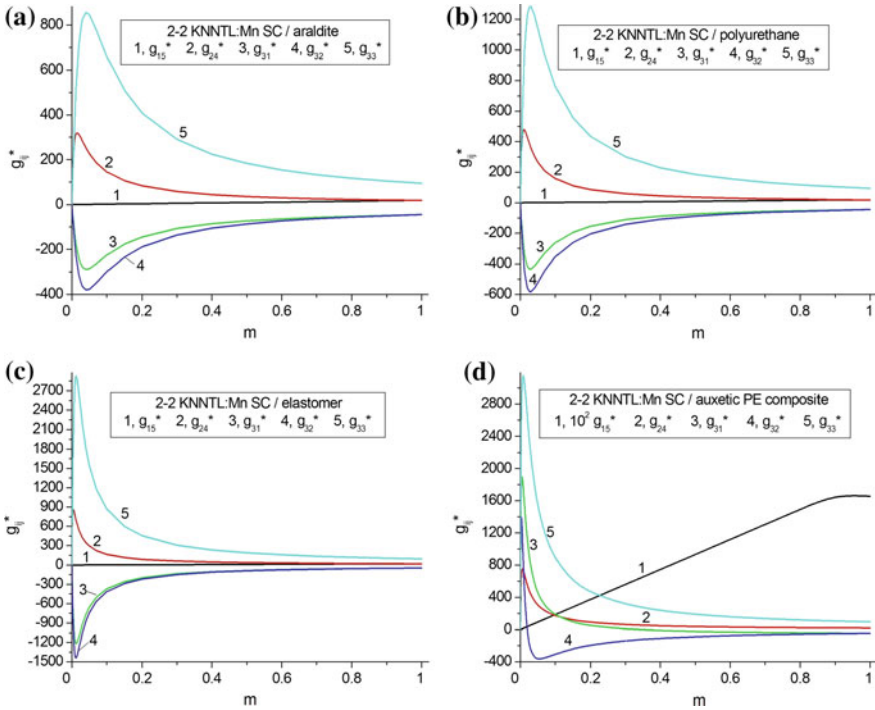


Fig. 3.1 Volume-fraction dependences of piezoelectric coefficients g_{ij}^* (in mV m/N) of 2–2 [001]-poled KNNTL:Mn SC/polymer composites. The schematic of the composite is shown in Fig. 2.2

values of the piezoelectric coefficients g_{24}^* and g_{3j}^* can be varied in wide ranges (see Fig. 3.1) mainly due to changes in the piezoelectric coefficients $d_{24}^{*σ}$ and $d_{3j}^{*σ}$ from (3.1). The dielectric permittivities $\epsilon_{22}^{*σ}$ and $\epsilon_{33}^{*σ}$ from (3.1) strongly influence g_{24}^* and g_{3j}^* at volume fractions of SC $m < 0.05$, i.e., in a volume-fraction range where the $\epsilon_{pp}^{*σ}$ values are comparable to the dielectric permittivity of the polymer component. Maxima and minima of g_{ij}^* (see curves 2–5 in Fig. 3.1) are observed at $m \ll 1$, where $|d_{ij}^{*σ}|$ increase rapidly, and the dielectric permittivities $\epsilon_{pp}^{*σ}$ exhibit a slow monotonic increase. A further increase of $|d_{ij}^{*σ}|$ at $m > 0.1$ becomes slow and cannot strongly influence the piezoelectric coefficients g_{ij}^* . The decrease in absolute values of g_{ij}^* becomes considerable at $m > 0.1$, when the dielectric permittivities $\epsilon_{pp}^{*σ}$ of the composite become large in comparison to ϵ_{pp} of the polymer component. We add that the similar volume-fraction behaviour of the piezoelectric coefficients g_{ij}^* is observed in 2–2 parallel-connected FC/polymer composites [7, 8, 14].

Of specific interest is the KNNTL:Mn SC/auxetic PE composite for which high PS and large values of $|g_{ij}^*|$ are predicted in Fig. 3.1d. At $m < 0.1$, we observe non-monotonic $g_{ij}^*(m)$ dependences that differ from those in the related composites (cf., for instance, Fig. 3.1c, d). This is accounted for by the active influence of the

elastic properties of the auxetic polymer component on the piezoelectric response of the composite, especially at large volume fractions of the polymer component. Such a trend was also observed and analysed in a case of the polarisation orientation effect in the 2–2-type composites [11].

Modifications of the 2–2 composite structure shown in Fig. 2.2 enable us to improve specific parameters of the studied composites. These modifications are concerned with the presence of inclusions in the polymer layers. For instance, a 2–2–0 composite with porous polymer layers is of interest due to increasing its hydrostatic parameters [12] in comparison to those of the related 2–2 composite. A 2–0–2 SC/FC/polymer composite studied in recent work [13] is also characterised by large hydrostatic parameters. Our next example is concerned with the PS of a 2–0–2 lead-free composite with two SC components.

It is assumed that the 2–0–2 composite consists of a system of parallel-connected layers of two types (*Type I* and *Type II* layers) with interfaces that are parallel to the (X_2OX_3) plane. The similar composite structure is shown in Fig. 2.8. The composite layers are regularly arranged along the coordinate OX_1 axis. The Type I layer is a domain-engineered SC and is characterised by a spontaneous polarisation $P_s^{(1)}$ and volume fraction m , and the main crystallographic axes of this SC are oriented as follows: X \parallel [001] \parallel OX_1 , Y \parallel [010] \parallel OX_2 and Z \parallel [001] \parallel OX_3 . Here the $[hkl]$ direction is given in the perovskite unit-cell axes. The Type II layer is a piezoelectric SC/polymer medium with 0–3 connectivity, and the volume fraction of the Type II layers is $1 - m$. The shape of each inclusion is shown in the inset of Fig. 2.8 and obeys (2.13) in the co-ordinate OX_f axes. Hereby $\rho_i = a_i/a_3$ is the aspect ratio of the SC inclusion, and m_i is the volume fraction of the SC inclusions in the Type II layer. The linear sizes of each SC inclusion in the Type II layer are much smaller than the thickness of each layer of the composite sample. The SC inclusions in the Type II layer occupy sites of a simple tetragonal lattice with unit-cell vectors parallel to the OX_f axes. The orientation of the crystallographic axes X, Y and Z of each SC inclusion in the Type II layer is given by X \parallel OX_1 , Y \parallel OX_2 and Z \parallel OX_3 .

The effective electromechanical properties of the aforementioned 2–0–2 composite are evaluated in two stages as described in Sect. 2.1.3. Among the lead-free components of interest, we consider the [001]-poled KNNTL:Mn SC in the Type I layer, a piezoelectric $\text{Li}_2\text{B}_4\text{O}_7$ (LBO) SC as an inclusion material in the Type II layer, and monolithic PE and polyurethane as matrix materials in the Type II layer. The full set of electromechanical constants of the LBO SC is shown in Table 3.1. We note that the LBO SC is a highly original component to use in a composite for the following reasons. For instance, the symmetry of the LBO SC in the Type II layer coincides with the macroscopic symmetry of the [001]-poled KNNTL:Mn SC in the Type I layer. The signs of the piezoelectric coefficients e_{ij} of the LBO SC (see Table 3.1) coincide with the signs of e_{ij} of the highly anisotropic PbTiO_3 -type FCs [16, 17], however the piezoelectric effect in the LBO SC is weaker than that in the poled PbTiO_3 -type FCs. The LBO SC is characterised by a considerable elastic anisotropy (Table 3.1), and the large ratio $c_{13}^E/c_{12}^E \approx 9.4$ has no analogies with other FCs and SCs.

Table 3.1 Room-temperature elastic moduli c_{ab} (in 10^{10} Pa), piezoelectric coefficients e_{ij} (in C/m²) and dielectric permittivity ϵ_{pp}^{ϵ} of the LBO SC, $4mm$ symmetry [15]

c_{11}^E	c_{12}^E	c_{13}^E	c_{33}^E	c_{44}^E	c_{66}^E	e_{31}	e_{33}	e_{15}	$\epsilon_{11}^{\epsilon}/\epsilon_0$	$\epsilon_{33}^{\epsilon}/\epsilon_0$
13.5	0.357	3.35	5.68	5.85	4.67	0.290	0.928	0.472	8.90	8.07

In the presence of the two SC components, that belong to the $4mm$ symmetry class, and an isotropic polymer component, the 2–0–2 composite is described by $mm2$ symmetry. Examples of the dependence of the piezoelectric coefficients g_{3j}^* of the 2–2–0 SC/SC/polymer composite on the volume fractions m and m_i and aspect ratio ρ_i are shown in Fig. 3.2.

As follows from Fig. 3.2a–c, the effect of the aspect ratio ρ_i of the SC inclusions on the PS is appreciable, even at relatively small volume fractions of the KNNTL: Mn SC ($m \leq 0.2$) and LBO SC ($m_i = 0.1$). The small values of the volume fractions m and m_i enable the composite to achieve large absolute values of g_{3j}^* , see Fig. 3.2a–c. A non-monotonic dependence of g_{3j}^* on ρ_i is observed in Fig. 3.2a–c at $0 < \rho_i < 3$, i.e., in the region where the elastic compliances of the Type II layer undergo large changes. Differences between ming_{31}^* (Fig. 3.2a) and ming_{32}^* (Fig. 3.2b) are accounted for by the role of the composite interfaces $x_1 = \text{const}$ (see Fig. 2.8). The interfaces influence the piezoelectric effect concerned with g_{31}^* to a larger extent in comparison to the piezoelectric effect concerned with g_{32}^* . As a consequence, the depth of ming_{31}^* is larger than that of ming_{32}^* (cf. Fig. 3.2a, b), however values of $|g_{31}^*|$ near ming_{31}^* are smaller than values of $|g_{32}^*|$ near ming_{32}^* . The sequence of curves 1–4 in Fig. 3.2a–c is related to the strong influence of the SC component in the Type I layer (main piezoelectric component) on the PS. On increasing the volume fraction m , $|g_{3j}^*|$ and PS decrease at $\rho_i = \text{const}$ and $m_i = \text{const}$. This occurs mainly because of the large dielectric permittivity $\epsilon_{33}^{(1),\sigma}$ of the Type I layer in comparison to $\epsilon_{33}^{(2),\sigma}$ of the Type II layer.

The LBO SC can influence an anisotropy of the piezoelectric coefficients g_{3j}^* , especially at $\rho_i \gg 1$. This is due to the influence of the elastic anisotropy of the Type II layer on the piezoelectric properties of the composite, and the similar effect was discussed in Sect. 2.1.3. On comparing the graphs in Fig. 3.2d, e, we conclude that the piezoelectric coefficient g_{33}^* is smaller at $m = \text{const}$ and $m_i = \text{const}$ for the polyurethane-containing composite. The polymer matrix with the smaller elastic compliances s_{ab} (i.e., PE in comparison to polyurethane, see data in Table 2.1) leads to a stiffer Type II layer which leads to a decrease in the PS of the composite as a whole.

The studied 2–0–2 KNNTL:Mn SC/LBO SC/PE composite has obvious advantages over various FCs and piezo-active composites. For instance, a nanostructured Mn-modified $(\text{K}_{0.5}\text{Na}_{0.5})\text{NbO}_3$ polycrystalline FC is characterised [18] by the piezoelectric coefficient $g_{33} = 220$ mV m/N. The piezoelectric coefficient $d_{33} = 340$ pC/N of the Mn-modified $(\text{K}_{0.5}\text{Na}_{0.5})\text{NbO}_3$ FC is comparable to d_{33}^* of the 2–0–2 composite, however the piezoelectric coefficient g_{33}^* of the

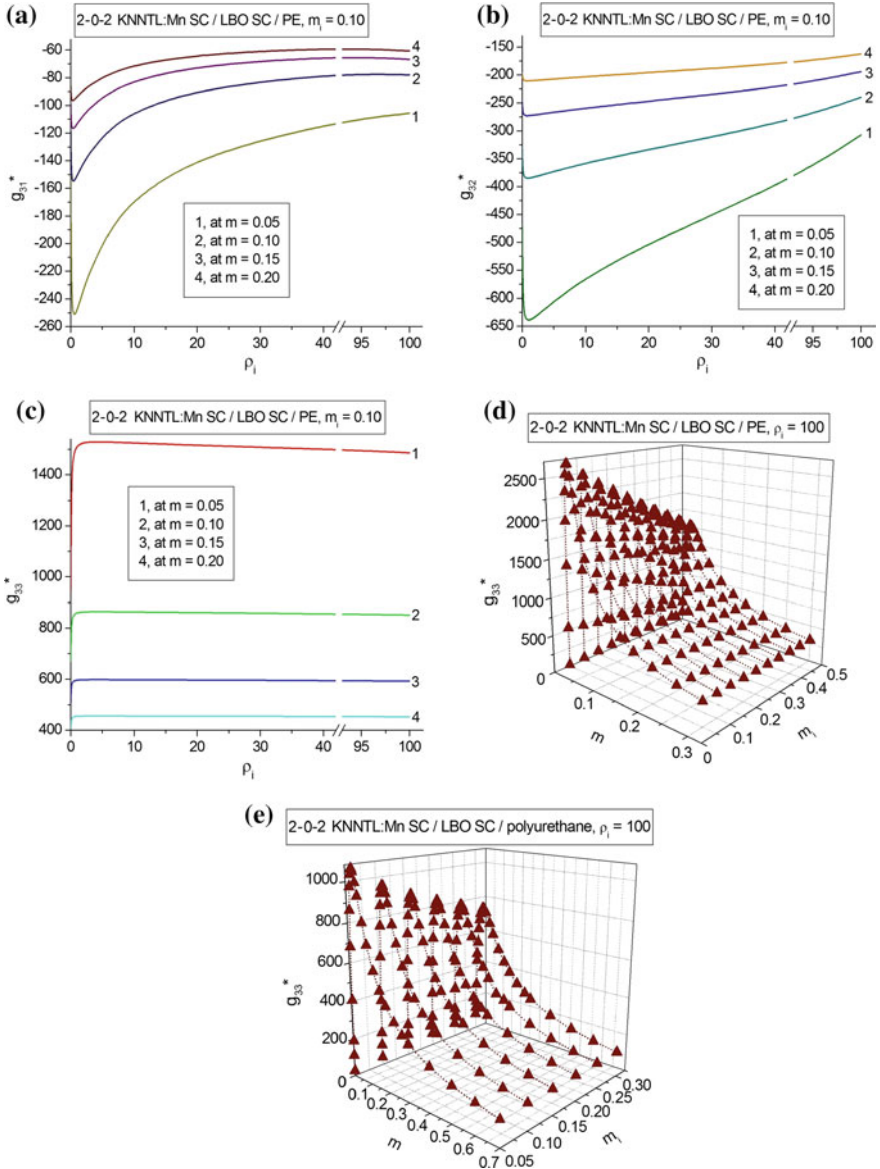


Fig. 3.2 Aspect-ratio (ρ_i) and volume-fraction (m and m_i) dependences of piezoelectric coefficients g_{ij}^* (in mV m/N) of the 2–0–2 [001]-poled KNNTL:Mn SC/LBO SC/PE composite (a–d) and 2–0–2 [001]-poled KNNTL:Mn SC/LBO SC/polyurethane composite (e)

aforementioned FC is smaller than g_{33}^* of the composite (see Fig. 3.2c, d). A novel grain-oriented and highly textured modified PbTiO_3 material was manufactured recently [19], and its piezoelectric coefficient $g_{33} = 115$ mV m/N is also smaller

than g_{33}^* of the studied 2–0–2 composite. In a 2–2 [111]-poled PMN–0.33PT SC/PVDF composite [20], the value of $\max g_{33}^* = 539 \text{ mV m/N}$ is comparable to $\max g_{33}^* = 605 \text{ mV m/N}$ related to a 2–2 [001]-poled PMN–0.33PT SC/PVDF composite.

Our further comparison of the PS and piezoelectric coefficients g_{ij}^* is concerned with composites based on the domain-engineered PMN– x PT SCs. In Table 3.2 we show data on g_{ij}^* of some composites whereby the SC component is poled along either the [001] or [011] direction in the perovskite unit cell. These results obtained within the framework of the matrix method suggest that the PS of the PMN–0.33PT-based composite is higher than the PS of the related PMN–0.28PT-based

Table 3.2 Piezoelectric coefficients g_{ij}^* (in mV m/N) of 2–2 parallel-connected composites based on PMN– x PT SCs

Polymer	m	g_{31}^*	g_{32}^*	g_{33}^*	g_{15}^*	g_{24}^*
<i>[001]-poled PMN–0.33PT SC/polymer</i>						
Elastomer	0.05	–314	–339	722	0.516	190
	0.10	–163	–177	376	1.03	99.1
	0.15	–111	–119	254	1.55	67.0
	0.20	–84.0	–90.2	191	2.06	50.6
Auxetic PE	0.05	242	–31.5	660	0.516	176
	0.10	87.1	–81.4	355	1.03	95.6
	0.15	42.4	–75.0	244	1.55	65.5
	0.20	22.1	–65.3	186	2.06	49.8
<i>[001]-poled PMN–0.28PT SC/polymer</i>						
Elastomer	0.05	–196	–225	463	0.412	152
	0.10	–102	–115	238	0.824	79.2
	0.15	–68.9	–77.3	160	1.24	53.6
	0.20	–52.3	–58.2	121	1.65	40.5
Auxetic PE	0.05	153	–47.7	450	0.412	140
	0.10	52.8	–63.4	234	0.824	76.0
	0.15	25.1	–53.9	158	1.24	52.2
	0.20	12.7	–45.3	120	1.65	39.7
<i>[011]-poled PMN–0.28PT SC/polymer</i>						
Elastomer	0.05	116	–600	465	2.88	300
	0.10	68.2	–318	242	5.77	159
	0.15	49.1	–216	164	8.65	108
	0.20	39.0	–164	124	11.5	81.7
Auxetic PE	0.05	–25.1	–470	390	2.88	284
	0.10	–19.5	–281	221	5.77	154
	0.15	–5.86	–200	154	8.65	106
	0.20	–1.14	–155	119	11.5	80.7

composite, and in both composite systems the SC component is [001]-poled. The larger $|g_{ij}^*|$ values are attained due to the larger $|d_{ij}|$ values of the SC component; see Tables 1.3 and 1.4. For example, the inequality $|g_{32}^*| > g_{33}^*$ holds in the composites based on the [011]-poled PMN–0.28PT SC. As follows from Table 1.4, the piezoelectric coefficients d_{3j} of this SC obey the condition $|d_{32}| > d_{33}$.

On increasing m , the considerable decrease of the $|g_{ij}^*|$ values of the composites listed in Table 3.2 is a result of the monotonic increase of the dielectric permittivities $\epsilon_{pp}^{*\sigma}$ and the slow increase of $|d_{ij}^*|$ at $m > 0.05$. We remind the reader that the piezoelectric coefficients g_{ij}^* of the 2–2-type composites listed in Table 3.2 obey (3.1). The use of an auxetic polymer component influences sgng_{31}^* , irrespective of the SC component. A change in sgng_{31}^* is also accounted for by a change in the poling direction of the SC component, which is seen in Table 3.2 for composites based on the [001]- and [011]-poled PMN–0.28PT SCs. It should be added that the g_{33}^* values shown in Table 3.2 are comparable to those of the 2–2 KNNTL:Mn SC/araldite composite (see curve 5 in Fig. 3.1a). As can be seen from Table 2.1, araldite has the lowest elastic compliances $|s_{ab}|$ among the polymer components and cannot achieve a high PS for the composite. However such shortcomings can be compensated by use of a KNNTL:Mn SC with large $|g_{3j}|$ values, and we see a number of examples of a high PS of the KNNTL:Mn-based composites in Fig. 3.1.

3.2 1–3-Type Composites

The 1–3 composite structure has been widely studied for PS and exhibits relations between the piezoelectric performance of the composite and its components [7–9, 21–29]. In the 1–3 composite shown in Fig. 2.11, C1 is a component with a high piezoelectric activity, and this component is self-connected in one dimension, often along the poling axis of the composite sample. C2 a component with a low piezoelectric activity or a piezo-passive component, and it is self-connected in three dimensions. A further modification of the composite structure is concerned with a formation of a porous polymer matrix, heterogeneous FC/polymer or SC/polymer matrix, laminar polymer matrix, etc. [23, 24, 28, 29]. In these cases we consider the 1–3-type composite keeping in mind that the system of long parallel rods represent the main piezoelectric component therein; see C1 in Fig. 2.11. In Sect. 3.2 we discuss examples of the behaviour of the piezoelectric coefficients g_{ij}^* of some 1–3-type composites on the assumption that a regular distribution of components over a composite sample is observed.

The graphs in Fig. 3.3 show that maxima or minima of g_{3j}^* are observed at volume fractions of SC $m \ll 1$. Moreover, values of $\max g_{33}^*$ related to composites with a non-auxetic polymer components are approximately equal to the $\max g_{33}^*$ values of the related 2–2 composites. This can be seen by comparing curve 3 in Fig. 3.3a–c and curve 5 in Fig. 3.1a–c. Minor differences between the $\max g_{33}^*$ values are a result of the analogous conditions for the longitudinal piezoelectric

response in the 2–2 parallel-connected (Fig. 2.2) and 1–3 (Fig. 2.11) composites. The auxetic polymer component strongly influences the piezoelectric response of these composites, especially at $0 < m < 0.02$, and we do not pay attention to these details here because of the very small volume fractions of SC m . It is also seen from Fig. 3.3 that $\max g_{33}^*$ and $\min g_{31}^*$ are observed at similar volume fractions and the difference is very small, as a rule, less than 0.01. This feature is due to the columnar structure of the 1–3 composite (Fig. 2.11) and due to the similar influence of the dielectric permittivity $\varepsilon_{pp}^{*\sigma}$ on g_{31}^* and g_{33}^* in accordance with (3.1). As with 2–2 composites, the 1–3 composites are characterised by relatively small values of g_{15}^* in a wide volume-fraction range, see curve 1 in Fig. 3.3. The interfaces that separate the C1 and C2 components in the 1–3 composite shown in Fig. 2.11 impede the shear piezoelectric response and lead to the ‘sleeping PS’, i.e., the piezoelectric coefficient g_{15}^* remains relatively small in comparison to $|g_{3j}^*|$ in the wide volume-fraction range. A similar situation concerning the small piezoelectric coefficient d_{15}^* was discussed in Sect. 2.2 on the 1–3-type composites, see also curves 1 in Figs. 2.12 and 2.16. Softening the polymer component in the 1–3 composite leads to the larger values of $|g_{3j}^*|$ for $m = \text{const}$, especially at $m \ll 1$,

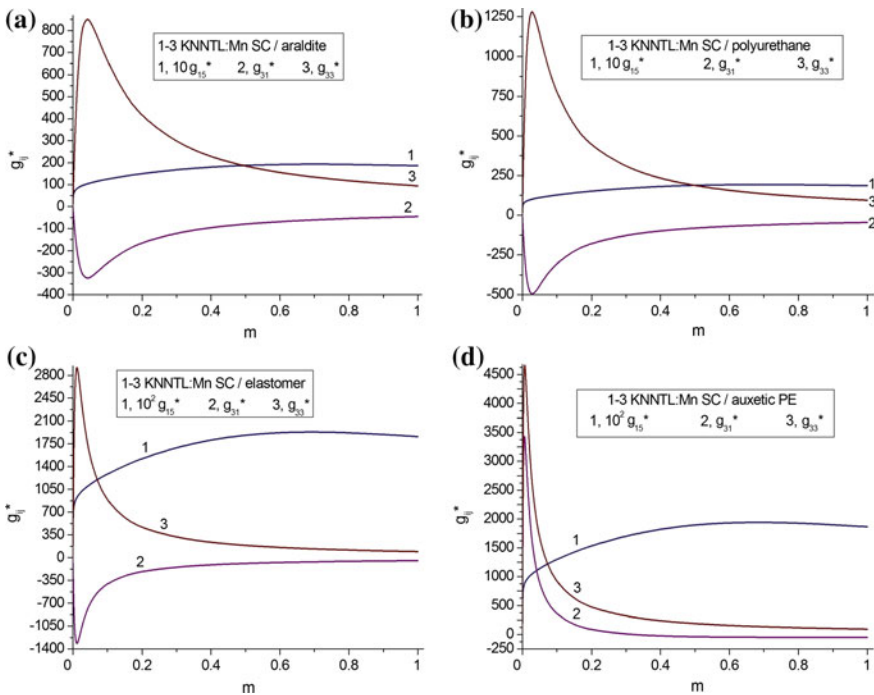


Fig. 3.3 Volume-fraction dependences of piezoelectric coefficients g_{ij}^* (in mV m/N) of 1–3 [001]-poled KNNTL:Mn SC/polymer composites. The schematic of the composite is shown in Fig. 2.11

however the extremum points of $g_{3j}^*(m)$ shift towards smaller volume fractions m (Fig. 3.3).

The next important example of large values of $|g_{3j}^*|$ is concerned with a 1–0–3 SC/FC/composite (see the schematic in Fig. 2.21) that was considered in Sect. 2.2.5. As in Sect. 2.2.5, we neglect the piezoelectric activity of the 0–3 FC/polymer matrix in comparison to the piezoelectric activity of the SC rods and consider the FC inclusions to be in an unpoled state. Elastic and dielectric properties of the 0–3 matrix influence the piezoelectric coefficients g_{ij}^* of the composite (Table 3.3) in a wide aspect-ratio (ρ_i) range even at relatively small volume fractions of FC m_i . Changes in g_{3j}^* are concerned with the large changes in the $s_{11}^{(0-3)}/s_{33}^{(0-3)}$ ratios (Table 2.4) during a transition from a prolate ($0 < \rho_i < 1$) to an oblate ($\rho_i > 1$) shape of the FC inclusion in the 0–3 matrix. Moreover, its dielectric permittivity $\varepsilon_{33}^{(0-3)}$ decreases on increasing ρ_i at $m_i = \text{const}$, and this decrease becomes a stimulus to increase g_{33}^* , especially at $m \ll 1$.

In contrast to g_{3j}^* , the piezoelectric coefficient g_{15}^* remains small and almost independent of the aspect ratio at ρ_i at $m_i = \text{const}$ (see Table 3.3), i.e., we observe a shear ‘sleeping PS’ by analogy with the case of 1–3 composites. We remember that the similar conditions (2.17) were formulated for the piezoelectric coefficients d_{ij}^* of the 1–3 composite. The shear ‘sleeping PS’ of the 1–0–3 composite is a result of its microgeometry (Fig. 2.11), namely, the system of interfaces $x_1 = \text{const}$ and $x_2 = \text{const}$ which separate the SC rod and surrounding 0–3 matrix and, therefore, impede the shear piezoelectric response to a certain extent.

As seen from Table 3.3, the piezoelectric coefficients g_{3f}^* at $\rho_i \geq 5$ and relatively small volume fractions m obey the condition

$$g_{33}^*/|g_{3f}^*| \geq 5 \quad (3.2)$$

that characterises the large piezoelectric anisotropy of the studied 1–0–3 composite, where $f = 1$ and 2. The condition (3.2) is to be taken into account at the prediction of the hydrostatic piezoelectric response, figures of merit, transducer characteristics [7, 8, 28–31], etc.

In the case of a 1–3–0 composite with a porous 3–0 matrix (Fig. 2.19), we also achieve large values of g_{3j}^* and small values of g_{15}^* (Table 3.4). The highly oblate shape of the air pores in the polymer matrix (i.e., $\rho_p \gg 1$) is more preferable to achieve a high longitudinal PS, or large values of g_{33}^* , at the valid condition (3.2) for the large anisotropy of g_{3j}^* . The system of highly oblate pores in the polymer matrix of the composite shown in Fig. 2.19 leads to a considerable elastic anisotropy of the matrix [29, 32], and this anisotropy promotes a certain weakening of the transverse PS and validity of the condition (3.2) across a wider m range in comparison to the aforementioned 1–0–3 composite. Due to the large piezoelectric coefficient d_{33} of the PMN–0.33PT SC (see Table 1.3), the values of $d_{33}^* \sim 10^3$ pC/N are typical for the studied 1–3–0 composite at $m > 0.05$, and we attain a good combination of

Table 3.3 Piezoelectric coefficients g_{ij}^* (in mV m/N) of the 1–0–3 [001]-poled KNNTL:Mn SC/modified PbTiO_3 (I) FC/monolithic PE composite with square cross section rods at $m_i = 0.1$

ρ_i	m	g_{31}^*	g_{33}^*	g_{15}^*
0.1	0.05	–214	864	11.4
	0.10	–179	677	13.0
	0.15	–145	519	14.3
	0.20	–123	415	15.4
0.5	0.05	–342	1430	11.4
	0.10	–216	840	13.0
	0.15	–161	588	14.3
	0.20	–131	451	15.4
1	0.05	–349	1490	11.4
	0.10	–216	856	13.0
	0.15	–160	594	14.3
	0.20	–130	454	15.3
2	0.05	–339	1520	11.4
	0.10	–209	862	13.0
	0.15	–155	597	14.2
	0.20	–126	45	15.3
5	0.05	–305	1530	11.3
	0.10	–191	864	12.9
	0.15	–144	598	14.2
	0.20	–118	456	15.3
10	0.05	–265	1530	11.1
	0.10	–170	864	12.8
	0.15	–131	598	14.1
	0.20	–109	456	15.2
100	0.05	–131	1510	10.1
	0.10	–102	858	11.9
	0.15	–88.4	594	13.3
	0.20	–79.9	454	14.5

large d_{33}^* and g_{33}^* values, i.e., the high level of the longitudinal PS is achieved. As follows from Table 3.4, changes in the porosity m_p of the matrix lead to minor changes in g_{ij}^* of the composite, and the latter changes are mainly due to a small decrease of the dielectric permittivity $\epsilon_{33}^{(3-0)}$ of the porous matrix on increasing m_p at $\rho_p = \text{const}$. The set of g_{3j}^* from Table 3.4 is to be taken into account at the analysis of the hydrostatic PS, figures of merit and ECFs.

Table 3.4 Piezoelectric coefficients g_{ij}^* (in mV m/N) of the 1–3–0 [001]-poled PMN–0.33PT SC/porous polyurethane composite with square cross section rods

ρ_p	m_p	m	g_{31}^*	g_{33}^*	g_{15}^*
0.1	0.1	0.05	-201	528	6.34
		0.10	-124	320	7.23
		0.15	-89.7	229	7.94
		0.20	-70.7	178	8.54
	0.2	0.05	-209	549	638
		0.10	-127	327	7.25
		0.15	-91.1	232	7.96
		0.20	-71.5	180	8.56
	0.3	0.05	-218	572	6.41
		0.10	-128	331	7.27
		0.15	-92.4	235	7.97
		0.20	-72.3	181	8.57
1	0.1	0.05	-201	543	6.34
		0.10	-122	325	7.23
		0.15	-88.4	231	7.94
		0.20	-69.6	179	8.54
	0.2	0.05	-212	585	6.37
		0.10	-124	335	7.25
		0.15	-88.5	236	7.95
		0.20	-69.4	182	8.55
	0.3	0.05	-245	689	6.41
		0.10	-125	344	7.27
		0.15	-88.6	240	7.97
		0.20	-69.2	184	8.57
100	0.1	0.05	-67.3	719	6.35
		0.10	-45.2	374	7.23
		0.15	-36.9	253	7.94
		0.20	-32.5	191	8.54
	0.2	0.05	-54.0	743	6.39
		0.10	-38.6	380	7.26
		0.15	-32.7	255	7.96
		0.20	-29.6	192	8.56
	0.3	0.05	-49.2	753	6.43
		0.10	-36.3	382	7.29
		0.15	-31.3	256	7.98
		0.20	-28.5	193	8.58

3.3 1–1-Type Composites

As is known from Sect. 2.3, the 1–1 FC/polymer composite (Fig. 2.25a) with the poling axis OX_3 and regular arrangement of components is characterised by $mm2$ symmetry. By analogy with (2.24), the piezoelectric coefficients g_{ij}^* of the 1–1 composite shown in Fig. 2.25a obey the condition

$$g_{ij}^*(t, n) = g_{ij}^*(1 - t, 1 - n) \quad (3.3)$$

Equations (3.1) are also valid for g_{ij}^* of the 1–1 FC/polymer composite poled along OX_3 . As with the 1–3 composite, the 1–1 composite is characterised by relatively small values of g_{15}^* because of the system of interfaces $x_1 = \text{const}$ and $x_2 = \text{const}$ (see Fig. 2.25a). The microgeometric analogy between the 1–3 and 1–1 composite structures (cf. Figs. 2.11 and 2.25a) suggests that large values of $|g_{3j}^*|$ are to be attained at volume fractions of FC $m \ll 1$: in this case the dielectric permittivity of the composite $\epsilon_{33}^{*\sigma}$ obeys the condition $\epsilon_{33}^{*\sigma} \ll \epsilon_{33}^{(1),\sigma}$ where $\epsilon_{33}^{(1),\sigma}$ is related to the FC component. The system of the long parallel FC rods poled along the OX_3 axis and the large volume fraction of the adjacent polymer rods in the 1–1 composite shown in Fig. 2.25a promote the large $|g_{3j}^*|$ values and high level of the PS.

The graphs in Fig. 3.4 show that the piezoelectric coefficients g_{3j}^* can be varied in a wide range, however these changes can be observed in a narrow range of the parameters t and n from (2.23). In fact, this can be considered a specific kind of the ‘sleeping PS’ in a composite structure with a complicated system of interfaces (Fig. 2.25a). In the case of an auxetic polymer matrix, changes in sgng_{31}^* and sgng_{32}^* are observed; see Fig. 3.4d, e. The sign-variable behaviour of g_{31}^* and g_{32}^* promote a validity of the condition (3.2), and the n and t ranges, wherein the condition (3.2) holds, depend on the elastic properties of the FC and polymer components. The considerable increase of $|g_{3j}^*|$ at $n \rightarrow 1$ and $t \rightarrow 0$ (Fig. 3.4) indicates that the condition $\epsilon_{33}^{*\sigma} \ll \epsilon_{33}^{(1),\sigma}$ holds, and the piezoelectric coefficients $|d_{3j}^*|$ show a large increase, see, e.g. Figure 2.26. A similar increase of $|g_{3j}^*|$ is achieved in the presence of the porous polymer matrix [33, 34] that surrounds the FC rods of the 1–1-type composite. Thus, the PS concerned with the piezoelectric coefficients g_{3j}^* of the 1–1-type composite depends on the elastic and dielectric properties of the polymer component to a large extent.

3.4 0–3-Type Composites

The 0–3 FC/polymer composite system is one of the most common composite types used for piezoelectric sensor applications [7, 9]. The 0–3 composite is schematically represented in Fig. 2.28. It is assumed that this composite consists of a

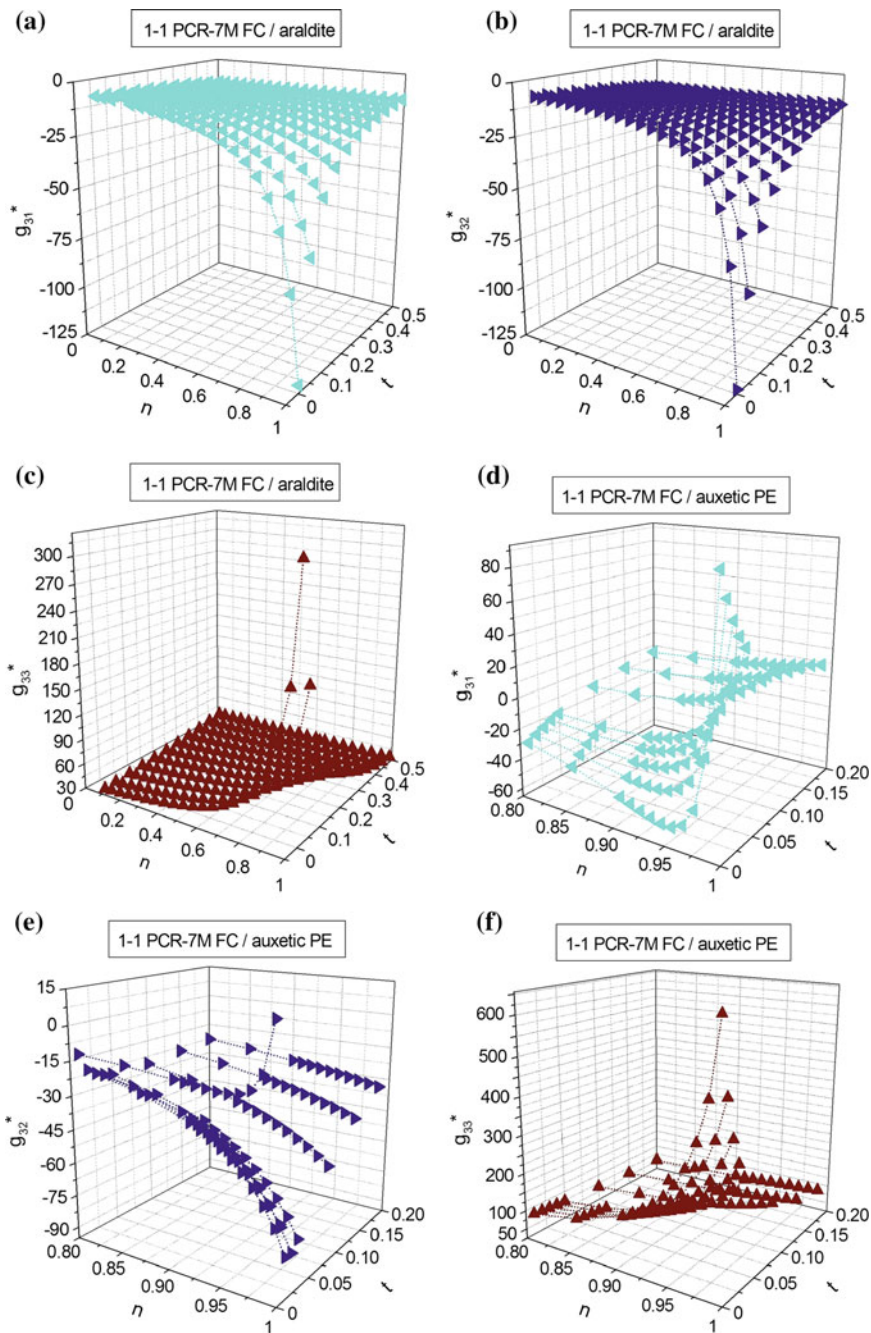


Fig. 3.4 Volume-fraction dependences of piezoelectric coefficients g_{ij}^* (in mV m/N) of 1–1 FC/polymer composites. The schematic of the composite is shown in Fig. 2.25a

three-dimensionally connected polymer matrix which is reinforced by a system of discrete FC inclusions, and the poling axis of the composite is OX_3 . The inclusions of the 0–3 composite are piezoelectric and distributed regularly throughout the sample. The shape of each inclusion is spheroidal and obeys (2.13). The centres of symmetry of the inclusions are located in apices of rectangular parallelepipeds and form a simple lattice. The matrix polymer component can be either piezo-active or piezo-passive. The next important kind of the 0–3 composite is the ferroelectric SC/polymer composite [7, 8].

As the effective parameters of the 0–3 composites are highly dependent [7, 9, 35–40] on their microstructure, properties and volume fractions of the components and poling conditions, the interrelations between the microgeometry and effective piezoelectric properties become complicated and require a careful and consistent physical interpretation. In Sect. 3.4 we discuss a number of examples of the PS and behaviour of the piezoelectric coefficients g_{ij}^* in 0–3-type composites that are based on either FCs or SCs.

Poled $(\text{Pb}_{1-x}\text{Ca}_x)\text{TiO}_3$ FCs are of interest (Table 3.5) due to their non-monotonic behaviour of both the piezoelectric anisotropy factors ($e_{33}/e_{31} > 0$ and $d_{33}/d_{31} < 0$) at molar concentrations $0.10 \leq x \leq 0.30$. Opposite signs of the piezoelectric coefficients e_{31} and d_{31} and minor changes in the piezoelectric coefficient g_{33} at changes in x (see Table 3.5) make these FCs unique and attractive components in the 0–3 composite, whose schematic structure is shown in Fig. 2.28.

The effective properties of the 0–3 $(\text{Pb}_{1-x}\text{Ca}_x)\text{TiO}_3$ FC/polymer composite are calculated in specific ranges of volume fractions m and aspect ratios ρ by means of FEM [8]. The calculated volume-fraction dependences of the piezoelectric coefficients g_{ij}^* are shown in Table 3.6. These dependences are similar to those determined by means of EFM [40] for the 0–3 $(\text{Pb}_{1-x}\text{Ca}_x)\text{TiO}_3$ -based composites with prolate FC inclusions, i.e., at $0 < \rho < 1$. As follows from Table 3.6, the piezoelectric coefficient g_{33}^* of the 0–3 composite can be over two times larger than the g_{33} value of the FC component, and minor differences between the $\max g_{33}^*$ values take place at $0.15 \leq x \leq 0.30$. The largest $\max g_{33}^*$ value is achieved at the volume fraction near $m = 0.10$ (see data for $x = 0.15$ in Table 3.6) that avoids potential technological problems when manufacturing the composite samples at a specific volume-fraction range. It is important that the piezoelectric coefficients g_{3j}^* of the composite obey the condition (3.2) for the large piezoelectric anisotropy because of the strong influence of the highly anisotropic FC component. We see from Table 3.6 that the piezoelectric coefficient g_{15}^* undergoes large changes on increasing the volume fraction of FC m , however the longitudinal PS remains higher than the shear PS in the whole m range. This is due to the highly prolate shape of the FC inclusion (i.e., the aspect ratio $\rho \gg 1$) and for the anisotropy of its piezoelectric properties (see the d_{33}/d_{31} ratios in Table 3.5).

The g_{33}^* values from Table 3.6 are smaller than the g_{33} value of a 0–3 PbTiO_3 FC/70/30 mol% copolymer of vinylidene fluoride and trifluoroethylene composite [43] and comparable to the g_{33}^* values of 0–3 composites [44–47] based on PZT-type FCs. The larger g_{33}^* values of the 0–3 composite from work [43, 44] may

Table 3.5 Calculated values of c_{ab}^E (in 10^{10} Pa), piezoelectric coefficients e_{ij} (in C/m²), relative dielectric permittivities $\epsilon_{pp}^{\epsilon}/\epsilon_0$, piezoelectric coefficient g_{33} (in mV m/N), and piezoelectric anisotropy factor d_{33}/d_{31} of the $(\text{Pb}_{1-x}\text{Ca}_x)\text{TiO}_3$ FC^a at room temperature (reprinted from Glushanin et al. [40], with permission from Elsevier)

x	c_{11}^E	c_{12}^E	c_{13}^E	c_{33}^E	c_{44}^E	e_{31}
0.10	19.1	5.22	5.15	18.6	6.85	0.676
0.15	18.8	5.09	5.01	18.3	6.76	0.751
0.20	18.5	4.76	4.68	18.0	6.79	0.844
0.23	18.7	5.03	4.93	18.2	6.76	1.06
0.24	18.4	4.72	4.61	17.9	6.76	1.07
0.25	18.9	5.19	5.06	18.3	6.76	1.33
0.26	18.9	5.14	5.02	18.3	6.77	1.36
0.30	18.6	4.89	4.80	18.1	6.77	1.08
x	e_{33}	e_{15}	$\epsilon_{11}^{\epsilon}/\epsilon_0$	$\epsilon_{33}^{\epsilon}/\epsilon_0$	g_{33}	d_{33}/d_{31}
0.10	3.90	1.62	111	109	21.1	-11.7
0.15	4.15	1.73	118	115	21.4	-13.0
0.20	4.31	1.77	126	123	20.6	-18.7
0.23	4.55	1.80	137	133	19.7	-30.3
0.24	4.69	1.87	145	141	19.4	-39.8
0.25	5.09	1.95	152	147	19.5	-71.9
0.26	5.30	2.03	161	156	19.1	-65.2
0.30	5.48	2.27	202	197	20.2	-17.6

^aThe full sets of electromechanical constants of poled FCs (∞mm symmetry) have been calculated by the effective medium method [41, 42]. It is assumed that spherical grains of the FC sample are split into 90° lamellar domains of two types with equal volume fractions, and these domains are separated by planar 90° domain walls. The 90° domain walls are assumed to be practically motionless so that a contribution from their displacements under external electric or mechanical fields into the electromechanical constants of the poled FC medium approaches zero [41, 42]. The electromechanical constants of the single-domain SC have been evaluated by the method put forward in work [41] on the basis of experimental room-temperature data on the ferroelectric $(\text{Pb}_{1-x}\text{Ca}_x)\text{TiO}_3$ solid solutions

be concerned with the presence of a ferroelectric polymer component and with a modification of the PbTiO_3 -type FC composition for improving the piezoelectric performance. At the same time, experimental g_{33}^* values related to a 0–3 PZT FC/PVDF composite manufactured by hot-pressing are approximately two–three times smaller [37] than g_{33}^* from Table 3.6. We remind the reader that according to data from Table 1.6, the PZT-type FCs are characterised by a piezoelectric coefficient g_{33} within the range from 14.3 to 49.0 mV m/N. As follows from Table 3.5 for various $(\text{Pb}_{1-x}\text{Ca}_x)\text{TiO}_3$ FCs, $g_{33} \approx 20$ mV m/N with the piezoelectric coefficient d_{33} being a few times smaller than the d_{33} of the PZT-type FCs listed in Table 1.5.

Thus, the longitudinal PS associated with the piezoelectric coefficient g_{33}^* of the 0–3 FC-based composites can be strongly dependent on the electromechanical properties of components and technological conditions for manufacturing. These

circumstances are to be taken into account along with the microgeometric features of the 0–3 composite structure.

An important example of the PS is concerned with a 0–3 lead-free SC/polymer composite that was highlighted in Sect. 2.4. In this lead-free composite we consider the prolate spheroidal SC inclusions poled along the OX_3 axis (Fig. 2.28) and compare the piezoelectric coefficients g_{3j}^* of such a composite to g_{3j}^* of the related 1–3 composite. It is assumed that in the 1–3 composite, the system of circular cylindrical SC rods are regularly distributed in the polymer matrix. Both the 0–3 and 1–3 composites based on SCs are characterised by a uniform orientation of the main crystallographic axes X, Y and Z in all of the SC inclusions (rods) as follows: $X \parallel OX_1$, $Y \parallel OX_2$ and $Z \parallel OX_3$. The graphs in Fig. 3.5 suggest that the transition from a 1–3 connectivity pattern to the 0–3 pattern leads to a drastic decrease of $|g_{3j}^*|$ in the whole volume-fraction range (cf., for instance, curves 1 and 2 in Fig. 3.5). Increasing the aspect ratio ρ in the range of $0 < \rho < 1$ leads to a considerable decrease of $\max g_{33}^*$ and $|\min g_{31}^*|$ and, therefore, to the weakening of the PS of the 0–3 composite. The main reason for such a decrease is due to a decrease of the piezoelectric coefficients $|d_{3j}^*|$ on increasing ρ at $m = \text{const}$. The use of less prolate piezoelectric inclusions with a larger ρ value in the 0–3 composite structure (Fig. 2.28) would lead to smaller values of $|d_{3j}^*|$ due to the strong influence of the depolarisation and elastic fields. However, despite the weakening of the PS due to the decrease of $|d_{3j}^*|$, the values of $|g_{3j}^*|$ of the KNNTL:Mn SC/polyurethane composite at $m = \text{const}$ (Fig. 3.5) remain larger than $|g_{3j}^*|$ of the 0–3 ($\text{Pb}_{1-x}\text{Ca}_x$) TiO_3 FC/araldite composite at $\rho = 0.1$ (Table 3.6). The large values of $|g_{3j}^*|$ of the 0–3 composite are due to the KNNTL:Mn SC component with large $|g_{3j}|$ values [48] and by the larger elastic compliances $|s_{ab}|$ of polyurethane in comparison to $|s_{ab}|$ of araldite (see Table 2.1).

Taking into account experimental data on PVDF (Table 3.7), we analysed the PS of the 0–3 and 1–3 KNNTL:Mn SC/PVDF composites at two different orientations

Table 3.6 Piezoelectric coefficients g_{ij}^* (in mV/mN)^a of the 0–3 ($\text{Pb}_{1-x}\text{Ca}_x$) TiO_3 FC/araldite composite at $\rho = 0.1$, FEM data

m	g_{31}^*	g_{33}^*	g_{15}^*									
	At $x = 0.15$			At $x = 0.20$			At $x = 0.25$			At $x = 0.30$		
0.05	-15.7	47.2	4.18	-15.8	46.2	4.00	-14.3	44.7	3.69	-12.9	39.2	3.25
0.10	-15.0	47.5	7.69	-14.3	46.4	7.35	-13.2	44.3	6.78	-11.9	38.5	5.96
0.15	-13.6	45.8	10.7	-12.9	44.6	10.2	-11.6	42.4	9.42	-10.6	36.6	8.28
0.20	-12.2	44.0	13.3	-11.5	42.8	12.7	-10.2	40.6	11.7	-9.41	34.9	10.3
0.30	-9.76	40.9	17.7	-9.06	39.8	16.9	-7.82	37.7	15.6	-7.39	32.3	13.7
0.40	-7.70	38.6	21.8	-7.02	37.5	20.9	-5.82	35.5	19.3	-5.71	30.3	16.9
0.50	-5.77	37.4	28.3	-5.11	36.4	27.2	-3.96	34.5	25.2	-4.16	29.4	22.3

^aThe values of g_{ij}^* have been calculated by using the full set of electromechanical constants (FEM data on s_{ab}^E , e_{ij}^* and ϵ_{pp}^S) of the 0–3 composite, see the schematic in Fig. 2.28

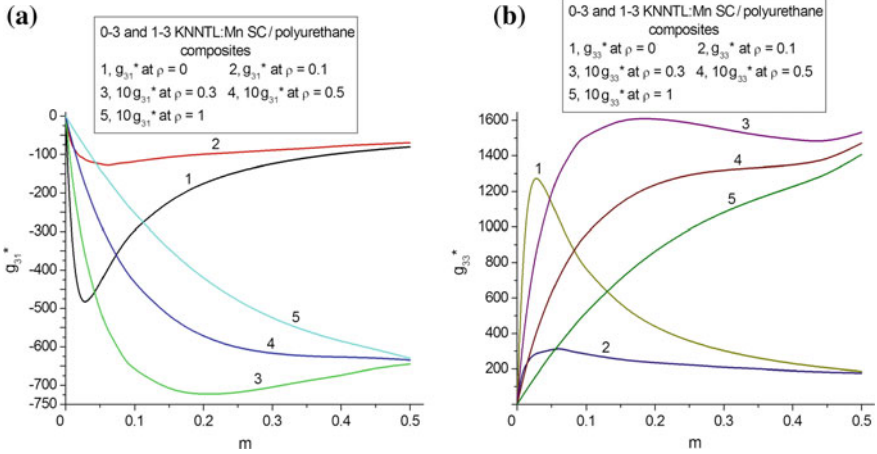


Fig. 3.5 Volume-fraction dependences of piezoelectric coefficients g_{3j}^* (in mV m/N) of 0-3 ($\rho > 0$) and 1-3 ($\rho = 0$) [001]-poled KNNTL:Mn SC/polyurethane composites, FEM data. The schematic of the 0-3 composite is shown in Fig. 2.28

of the remanent polarisation vector of PVDF (Table 3.8). The small piezoelectric coefficients e_{15} and e_{31} in comparison to $|e_{33}|$ of PVDF (see Table 3.7) and opportunities to pole the composite components in different directions [8, 35, 36, 49] make PVDF attractive as a ferroelectric polymer component. We remind the reader that the coercive field E_c of PVDF [50] is much larger than E_c of the KNNTL:Mn, PMN- x PT, PZN- x PT, and other important ferroelectric solid solutions [10, 48] in the SC state. As seen from Table 3.8, the PVDF matrix strongly influences the PS of the composites and enables us to observe a sign-variable behaviour of the piezoelectric coefficients g_{3j}^* at the relatively small volume fractions of SC m . This means that the conditions

$$g_{31}^* = 0 \text{ at } g_{33}^* \neq 0 \text{ or } g_{33}^* = 0 \text{ at } g_{31}^* \neq 0 \quad (3.4)$$

hold in specific ρ and m ranges which depend on the electromechanical properties and poling directions of the components. On varying ρ at $m = \text{const}$, we observe a unique ‘aspect-ratio effect’: both g_{31}^* and g_{33}^* demonstrate the non-monotonic

Table 3.7 Room-temperature elastic moduli c_{ab}^E (in 10^{10} Pa), piezoelectric coefficients e_{ij} (in C/m²) and relative dielectric permittivity $\epsilon_{pp}^E/\epsilon_0$ of poled PVDF [49] at the remanent polarisation $\mathbf{P}_r^{(2)} \uparrow \uparrow OX_3$

c_{11}^E	c_{12}^E	c_{13}^E	c_{13}^E	c_{44}^E	c_{66}^E
0.4840	0.2720	0.2220	0.4630	5.26×10^{-3}	0.1060
e_{15}	e_{31}	e_{33}	$\epsilon_{11}^E/\epsilon_0$	$\epsilon_{33}^E/\epsilon_0$	
1.999×10^{-3}	4.344×10^{-3}	-0.1099	7.504	8.003	

Table 3.8 Piezoelectric coefficients g_{3j}^* (in mV m/N)^a of 0–3 ($\rho > 0$) and 1–3 ($\rho = 0$) [001]-poled KNNTL:Mn SC/PVDF composites^b

ρ	g_{31}^*	g_{33}^*	g_{31}^*	g_{33}^*	g_{31}^*	g_{33}^*
	At $m = 0.05$		At $m = 0.10$		At $m = 0.15$	
<i>PVDF matrix with the remanent polarisation $\mathbf{P}_r^{(2)} \uparrow\uparrow OX_3$</i>						
0	-279	714	-210	657	-171	519
0.1	42.0	-183	2.89	-79.2	-183	-24.1
0.3	78.2	-292	41.4	-197	15.4	-130
0.5	94.8	-339	58.2	-245	31.0	-175
1	112	-387	80.1	-306	53.0	237
<i>PVDF matrix with the remanent polarisation $\mathbf{P}_r^{(2)} \uparrow\downarrow OX_3$</i>						
0	-253	812	-202	628	-163	490
0.1	-132	408	-119	363	-108	327
0.3	-126	395	-113	352	-104	320
0.5	-129	410	-116	366	-106	332
1	-134	431	-122	391	-112	358

^aThe values of g_{3j}^* have been calculated by using the full set of electromechanical constants (FEM data on s_{ab}^*E , e_{ij}^* and ϵ_{pp}^{*s}) of the composite

^bThe schematic of the 0–3 composite is shown in Fig. 2.28

behaviour (see Table 3.8), and this behaviour is due to the elastic and dielectric properties of the composite in the presence of the PVDF matrix with the dominating longitudinal piezoelectric effect.

Relations between the piezoelectric coefficients g_{3j}^* and d_{3j}^* of the 0–3 KNNTL:Mn SC SC/PVDF composite are shown in Fig. 3.6. As described previously, the piezoelectric coefficients g_{3j}^* and d_{3j}^* are linked by (3.1). A change in the aspect ratio ρ of the SC inclusion leads to a change in the anisotropy of g_{3j}^* and d_{3j}^* . On taking into account data from Figs. 3.5 and 3.6 and Table 3.8, we state that the larger changes in the piezoelectric coefficients g_{3j}^* are observed in the PVDF-containing composites. Moreover, the values of $|g_{3j}^*|$ in specific ranges of m and ρ are a few times larger than $|g_{3j}^*|$ of the 0–3 FC-based composites, see Table 3.6 and work [37, 40, 43–47].

The next example of the PS is related to the 0–3-type composite [51] with the porous polymer matrix. According to work [51], the system of spheroidal SC inclusions is surrounded by the porous polymer matrix, and the shape of each pore is spheroidal with the aspect ratio ρ_p . A regular arrangement of the inclusions and pores takes place over the whole composite sample. The polymer matrix with isolated pores is characterised by 3–0 connectivity while the composite as a whole is characterised by 0–3–0 connectivity. The effective electromechanical properties of the studied composite are evaluated in two stages. At the first stage, the properties of the 3–0 matrix are determined using (2.19). At the second stage, FEM is applied to attain the full set of electromechanical constants of the 0–3–0 composite. The highly oblate air pore strongly influences the elastic anisotropy of the matrix and the anisotropy of the piezoelectric coefficients g_{3j}^* of the composite. Figure 3.7

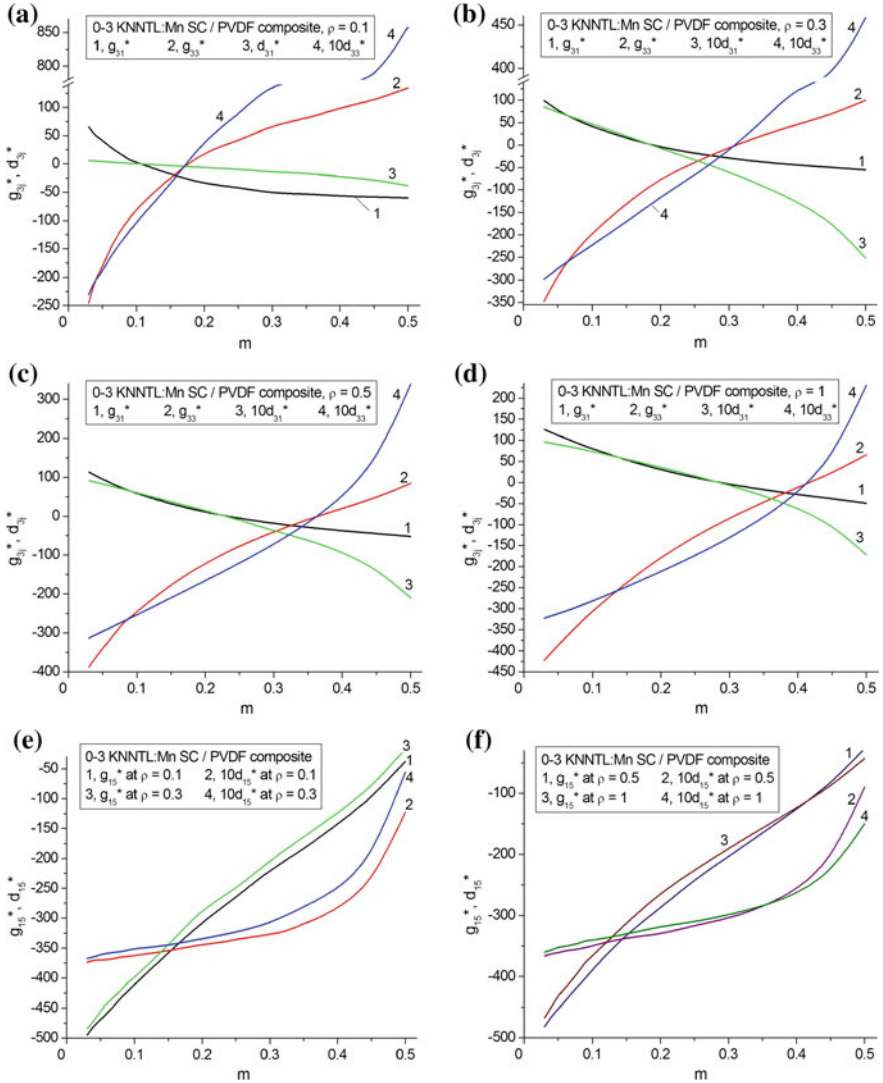
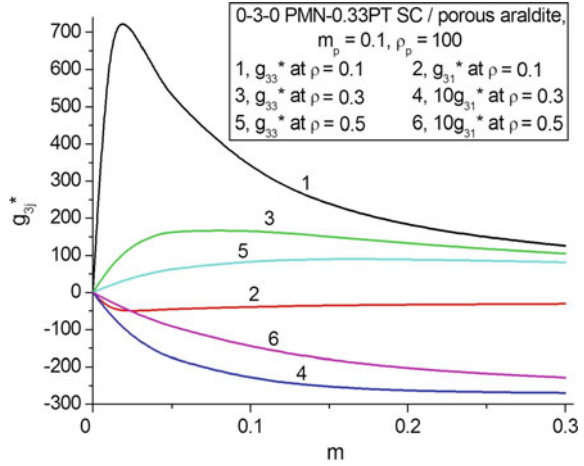


Fig. 3.6 Volume-fraction dependences of piezoelectric coefficients g_{ij}^* (in mV/mN) and d_{ij}^* (in pC/N) of the 0-3 [001]-poled KNNTL:Mn SC/PVDF composite with the remanent polarisation of the PVDF matrix $P_r^{(2)} \uparrow\uparrow OX_3$, FEM data. The schematic of the 0-3 composite is shown in Fig. 2.28

shows that even at relatively small porosity levels of the matrix ($m_p = 0.1$), large changes in g_{3j}^* are observed, and these changes are caused by changes in the volume fraction m and aspect ratio ρ of the SC inclusions. It is also seen from Fig. 3.7 that the piezoelectric coefficients g_{3j}^* obey (3.2) for a large anisotropy. The volume-fraction (m) range wherein the condition (3.2) is valid strongly depends on

Fig. 3.7 Volume-fraction dependences of piezoelectric coefficients g_{3j}^* (in mV m/N) of the 0–3–0 [001]-poled PMN–0.33PT SC/porous araldite composite (reprinted from paper by Topolov et al. [51], with permission from Taylor and Francis)



the aspect ratios ρ and ρ_p of the SC inclusion and pore, respectively, and on the porosity of the matrix m_p . The values of g_{3j}^* shown in Fig. 3.7 are comparable to those related to the 0–3 KNNTL:Mn SC/PVDF, see Table 3.8 and Fig. 3.6a–d.

In the next example of the PS we consider a SC-based composite wherein the matrix surrounding the SC inclusions is either monolithic FC or porous FC with 3–0 connectivity, and both components are poled along the OX_3 axis [52]. Table 3.9 shows the piezoelectric performance of the 0–3 and 0–3–0 composites with two relaxor-ferroelectric components. Hereby changes in the piezoelectric coefficients g_{ij}^* take place in relatively narrow ranges when the volume fraction of SC m is varied from 0.05 to 0.50. Both the SC and FC components are characterised by a similar anisotropy of the piezoelectric coefficients d_{3j} : according to data from Tables 1.3 and 1.5, $d_{33}/d_{31} = -2.12$ and -2.03 for the [001]-poled PMN–0.33PT SC and PMN–0.35PT FC, respectively. This feature does not promote a considerable anisotropy of g_{3j}^* in the composites, see Table 3.9. An increase of the aspect ratio ρ in both the 0–3 and 0–3–0 composites does not lead to appreciable changes in g_{ij}^* at $m = \text{const}$, and such a stability can be accounted for by the considerable elastic stiffness of the FC matrix. The formation of air pores in the FC matrix promotes an increase of $|g_{ij}^*|$ in comparison to the case of the 0–3 composite, see Table 3.9. This is due to a decrease of the dielectric permittivity of the porous FC matrix in comparison to the monolithic FC matrix. We add that the g_{33}^* values related to the 0–3 SC/FC composite (Table 3.9) are approximately equal to $\max g_{33}^* = 20$ mV m/N found for a 0–3 PMN FC/sulphoaluminate cement composite [53] wherein only the FC component exhibits the piezoelectric properties.

The numerous results on the PS of the 0–3-type composites make these materials attractive in sensor and related piezotechnical applications [2, 4, 9, 44], where flexible piezoelectric elements are required and the shape of the element can conform with the device configuration.

Table 3.9 Piezoelectric coefficients g_{ij}^* (in mV m/N) of 0–3 SC/FC and 0–3–0 SC/porous FC composites based on the [001]-poled PMN–0.33PT SC, FEM data

m	g_{31}^*	g_{33}^*	g_{15}^*	g_{31}^*	g_{33}^*	g_{15}^*	g_{31}^*	g_{33}^*	g_{15}^*
	At $\rho = 0.1$			At $\rho = 0.3$			At $\rho = 0.5$		
<i>0–3 PMN–0.33PT SC/PMN–0.35 FC^a</i>									
0.05	–5.83	12.7	21.5	–5.86	12.8	21.5	–5.88	12.9	21.6
0.10	–6.14	13.4	20.8	–6.19	13.5	20.8	–6.24	13.6	20.8
0.15	–6.47	14.1	20.1	–6.54	14.2	20.1	–6.61	14.4	20.1
0.20	–6.83	14.8	19.3	–6.91	15.0	19.3	–7.00	15.2	19.4
0.30	–7.63	16.5	17.9	–7.75	16.8	18.0	–7.87	17.0	18.0
0.40	–8.58	18.5	16.6	–8.72	18.8	16.6	–8.85	19.1	16.7
0.50	–9.69	20.8	15.4	–9.83	21.1	15.4	–9.96	21.4	15.4
<i>0–3–0 PMN–0.33PT SC/porous PMN–0.35 FC at $m_p = 0.3$ and $\rho_p = 1^b$</i>									
0.05	–8.74	21.4	31.9	–8.76	21.4	31.9	–8.79	21.2	31.9
0.10	–9.27	22.5	30.2	–9.31	22.5	30.2	–9.35	22.6	30.1
0.15	–9.82	23.6	28.5	–9.87	23.6	28.5	–9.93	23.7	28.4
0.20	–10.4	24.6	26.8	–10.4	24.7	26.8	–10.5	24.7	26.8
0.30	–11.5	26.8	23.8	–11.6	26.9	23.8	–11.7	26.9	23.8
0.40	–12.7	29.0	21.1	–12.8	29.1	21.1	–12.8	29.1	21.0
0.50	–13.9	31.2	18.6	–13.9	31.1	18.6	–13.9	31.1	18.5

^aThe schematic of the 0–3 composite is shown in Fig. 2.28

^bThe full set of electromechanical constants of the poled porous PMN–0.35PT FC has been found in work [52]

3.5 3– β Composites

In a composite with 3– β connectivity, the first component (main piezoelectric component) is distributed continuously along three co-ordinate axes, and the second component is distributed along β co-ordinate axes, where $\beta = 0, 1, 2,$ or 3 . Traditionally such composites contain FC and polymer components that are often distributed regularly [54, 55]. To the best of our knowledge, there are fairly restricted experimental data on the PS of the 3– β FC/polymer composites [44, 54, 55] and no papers where the four types of the piezoelectric coefficients, d_{ij}^* , e_{ij}^* , g_{ij}^* , and h_{ij}^* , were analysed.

In the first example, we consider the longitudinal PS that is described by the piezoelectric coefficient g_{33}^* . Its volume-fraction dependence (Fig. 3.8) was found based on experimental data on the piezoelectric coefficient d_{33}^* and dielectric permittivity $\epsilon_{33}^{*\sigma}$, see (3.1). As follows from Fig. 3.8, $\max g_{33}^*$ is achieved at a relatively large volume fraction of FC (i.e., $0.4 < m < 0.5$). To a large extent, the location of $\max g_{33}^*$ depends on dielectric and elastic properties of the components. The value of $\max g_{33}^*$ (Fig. 3.8) is comparable to experimental values of g_{33}^* related to some 0–3 PZT-type FC/polymer composites, see e.g. [45–47].

Fig. 3.8 Volume-fraction dependence of the piezoelectric coefficient g_{33}^* (in mV m/N) of the 3-3 PZT-5H FC/epoxy composite (evaluated from experimental data [54])

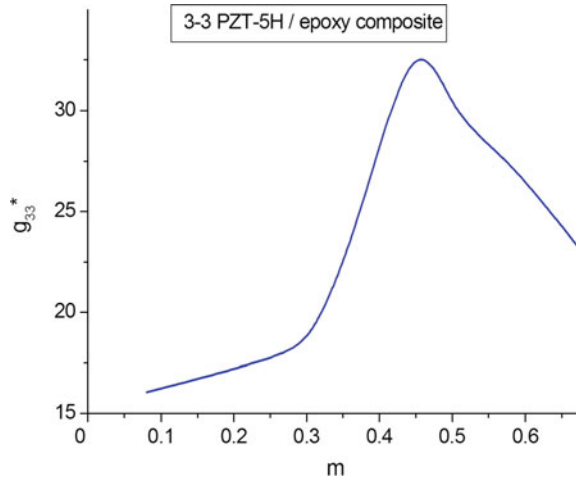
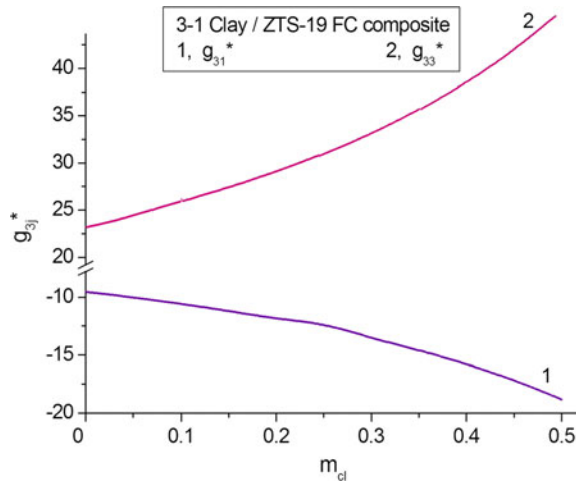


Fig. 3.9 Volume-fraction dependence of the piezoelectric coefficients g_{3j}^* (in mV m/N) of the 3-1 ZTS-19 FC/clay composite, FEM data



The second example is concerned with a 3-1 FC/clay composite wherein the system of circular cylinders (clay rods) are aligned parallel to the poling axis OX_3 , and centres of symmetry of bases of the cylinders form a square lattice on the (X_1OX_2) plane. It is assumed that the volume fractions of clay m_{cl} and FC m are linked by the equation $m_{cl} = 1 - m$. On increasing the volume fraction of clay m_{cl} , we observe a monotonic increase of $|g_{3j}^*|$, see Fig. 3.9. This increase is mainly due to the influence of the small dielectric permittivity ϵ_{pp} of clay on the effective properties of the composite. As for the elastic properties of clay, their influence on the piezoelectric coefficients g_{3j}^* of the composite is restricted because of the stiff FC matrix surrounding each clay rod in the 3-1 composite.

As with g_{33}^* of the 3–3 FC/polymer composite in Fig. 3.8, at equal volume fractions of components, the g_{33}^* value of the 3–1 FC/clay composite is approximately two times larger than g_{33} of the FC component (see data at $m_{cl} = 0$ and $m_{cl} = 0.5$ in Fig. 3.9). Such a similarity is observed in the presence of different FC components, PZT-5H and ZTS-19, however differences between their electromechanical properties (Table 1.5) are not very large. It should be added that the effective properties of the 3–1 composite were used for the interpretation of the piezoelectric performance of a ZTS-19 FC/clay composite [56].

3.6 Piezoelectric Sensitivity, Figures of Merit and Anisotropy

The relationships between the PS and squared figures of merit from (1.41) and (1.42) have been discussed in papers on piezo-active composites; see, for instance [9, 24, 26, 56, 57]. In Sect. 3.6 we show a few examples of the behaviour of the squared figures of merit related to the longitudinal and transverse PS of the composites. The squared figures of merit $(Q_{3j}^*)^2$ of the composite can be represented as

$$(Q_{3j}^*)^2 = d_{3j}^* g_{3j}^* = (g_{3j}^*)^2 \epsilon_{33}^{*\sigma} \quad (3.5)$$

in the case where the piezoelectric coefficients d_{3j}^* and g_{3j}^* are linked by the relation $d_{3j}^* = \epsilon_{33}^{*\sigma} g_{3j}^*$ [see (1.20)], where $j = 1, 2$ and 3 . Formula (3.5) suggests that large values of $(Q_{33}^*)^2$ can be achieved from large piezoelectric coefficient g_{33}^* . However, large g_{33}^* values are often related to relatively small volume fractions of the main piezoelectric component, and this is typical of various composites considered in this chapter; see, for instance, Figs. 3.1, 3.2, 3.3 and 3.4. At the small volume fractions of the main piezoelectric component, the dielectric permittivity $\epsilon_{33}^{*\sigma}$ of the composite remains small in comparison to that of the main piezoelectric component. Thus, there is a need to find a ‘compromise’ between the relatively large g_{33}^* values and moderate $\epsilon_{33}^{*\sigma}$ values in the composite. The squared figures of merit $(Q_{31}^*)^2$ and $(Q_{32}^*)^2$, which are concerned with the transverse piezoelectric effect, can be small [8, 58] in comparison to $(Q_{33}^*)^2$ to satisfy conditions for effective energy harvesting and transformation, or to achieve a considerable hydrostatic piezoelectric response, etc. As follows from (3.5), the condition

$$(Q_{33}^*)^2 \gg (Q_{3f}^*)^2 (f = 1 \text{ and } 2) \quad (3.6)$$

is linked with validity of (3.2), i.e., with the large piezoelectric anisotropy of the composite.

The first example of validity of (3.2) and (3.6) is concerned with the 1–3–0 SC/porous polymer composite whose structure is shown schematically in Fig. 2.19. As

in Sect. 2.2.4, a regular distribution of SC rods and air pores over the composite sample is assumed. The graphs in Fig. 3.10 have been built for volume fractions of SC $0.001 \leq m \leq 0.30$, since in this volume-fraction range there are extreme points of $(Q_{3j}^*)^2$ and appreciable changes in the anisotropy of g_{3j}^* , where $j = 1, 2$ and 3. Even at relatively small porosity levels for the polymer matrix ($m_p = 0.1$), the anisotropy of g_{3j}^* becomes higher on increasing the aspect ratio ρ_p of the air pores, see Fig. 3.10a. This highlights that the elastic anisotropy of the polymer matrix containing highly oblate pores (see the inset in Fig. 2.19) favours a validity of the condition (3.2), see curve 3 in Fig. 3.10. Differences between $(Q_{3j}^*)^2$ (see Fig. 3.10b, c) on variation of the volume fraction of SC m and the aspect ratio ρ_p of the air pores in the polymer matrix are mainly accounted for by the strong influence of the elastic anisotropy of the porous matrix on the PS of the composite.

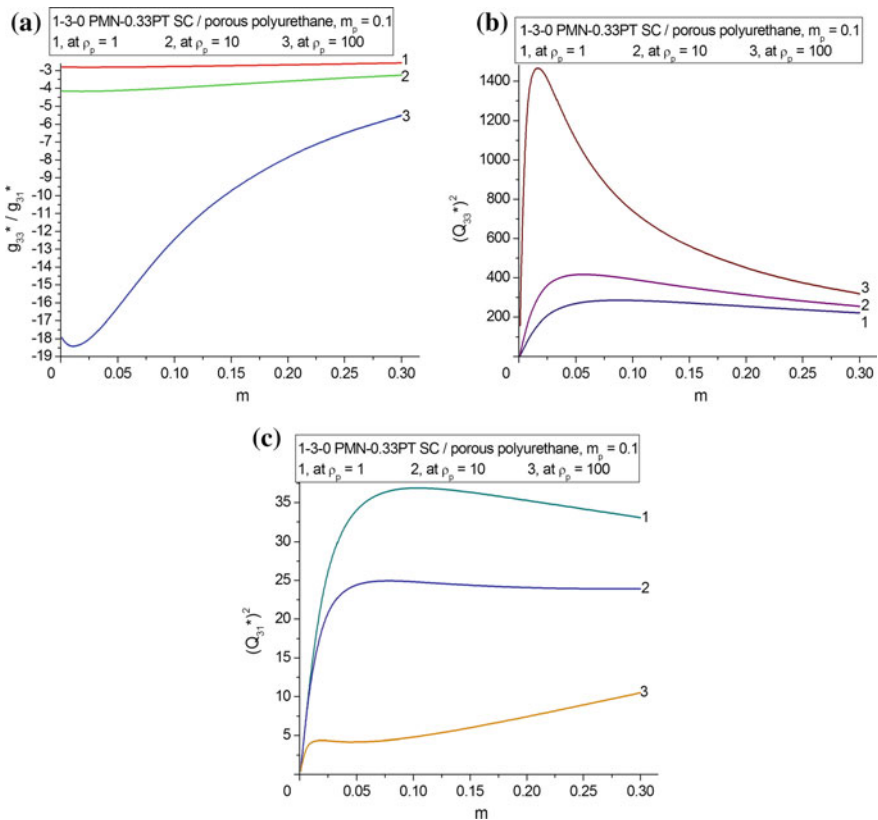


Fig. 3.10 Volume-fraction dependences of the anisotropy of piezoelectric coefficients g_{3j}^* (a) and squared figures of merit $(Q_{3j}^*)^2$ (b and c, in 10^{-12} Pa^{-1}) of the 1–3–0 [001]-poled PMN–0.33PT SC/porous polyurethane composite. The schematic of the composite is shown in Fig. 2.19

Our comparison of curves 1–3 in Fig. 3.10b, c enables us to state that the composite at $\rho_p = 100$ provides large values of $(Q_{33}^*)^2$ at validity of the condition (3.6) in the large volume-fraction (m) range. Large values of $(Q_{33}^*)^2$ are also achieved due to the relatively small $\varepsilon_{33}^{*\sigma}$ values of the composite in comparison to $\varepsilon_{33}^{(1),\sigma}$ of its SC component, and the $\varepsilon_{33}^{*\sigma}$ values are influenced by the aspect ratio ρ_p of the pore to a large extent. It should be added that the $(Q_{33}^*)^2$ values from Fig. 3.10b are one–two orders-of-magnitude larger than a value of $(Q_{33}^*)^2 = 17 \times 10^{-12} \text{ Pa}^{-1}$ for a perforated 1–3-type PZT FC/epoxy composite [57]. The advantage of the studied 1–3–0 PMN–0.33PT-based composite over the perforated 1–3-type PZT-based composite is primarily the large piezoelectric coefficient $d_{3j}^{(1)}$ of the [001]-poled PMN–0.33PT SC in comparison with $d_{3j}^{(1)}$ of poled PZT-type FCs, see Tables 1.3 and 1.5. The oblate shape of the air pores in the polymer matrix, see inset in Fig. 2.19, plays an important role in achieving a large piezoelectric anisotropy in the composite. For example, the condition (3.2) holds for the 1–3–0 PMN–0.33PT SC/porous polyurethane composite at an aspect ratio $\rho_p = 100$ in the following volume-fraction ranges of SC: $0 < m \leq 0.264$ (at $m_p = 0.1$), $0 < m \leq 0.294$ (at $m_p = 0.2$), and $0 < m \leq 0.304$ (at $m_p = 0.3$). This may be concerned with the active influence of the air pores on the dielectric and piezoelectric properties of the porous matrix and composite as a whole, and the use of a larger porosity level can promote a larger elastic anisotropy of the porous polymer matrix that strongly influences the PS of the composite.

In the second example we observe a large piezoelectric anisotropy in a 1–3-type composite (Table 3.10) whereby using an auxetic PE strongly influences the PS and leads to a change in sgng_{31}^* at a volume fraction of SC $0.30 < m < 0.35$. Hereby conditions (3.2) and (3.6) hold at large values of g_{33}^* and $(Q_{33}^*)^2$ in a relatively wide volume-fraction range, see data from the 5th and 7th columns in Table 3.10. The $(Q_{33}^*)^2$ value becomes smaller than $(Q_{33}^*)^2$ of the 1–3–0 PMN-0.33PT-based

Table 3.10 Piezoelectric coefficients d_{3j}^* (in pC/N) and g_{3j}^* (in mV m/N), and squared figures of merit $(Q_{3j}^*)^2$ (in 10^{-12} Pa^{-1}) of the 1–3-type [001]-poled PMN–0.28PT SC/auxetic PE composite^a in the region of the large piezoelectric anisotropy

m	d_{31}^*	d_{33}^*	g_{31}^*	g_{33}^*	$(Q_{31}^*)^2$	$(Q_{33}^*)^2$
0.20	190	1080	21.1	120	4.01	130
0.25	90.8	1100	7.98	96.5	0.725	106
0.30	5.11	1110	0.371	80.5	1.90×10^{-3}	89.4
0.35	–69.4	1120	–4.28	69.1	0.297	77.4
0.40	–135	1130	–7.22	60.6	0.975	68.5
0.45	–192	1140	–9.11	53.9	1.75	61.4

^aSee the schematic of the composite in Fig. 2.11. Calculations have been performed by means of FEM

composite, see Fig. 3.10b. This is due to smaller piezoelectric coefficients $d_{3j}^{(1)}$ of the [001]-poled PMN–0.28PT SC in comparison with $d_{3j}^{(1)}$ of the [001]-poled PMN–0.33PT SC, see data in Table 1.3. For instance, the piezoelectric coefficient $d_{33}^{(1)}$ of the PMN–0.28PT SC is approximately 2.4 times smaller than $d_{33}^{(1)}$ of the PMN–0.33PT SC.

The third example is concerned with the 1–3-type FC-based composite wherein the sgng_{31}^* changes with a change in the aspect ratio η of the FC rod in the form of an elliptical cylinder. We remind the reader that a similar 1–3-type composite was analysed in Sect. 2.2.1. In our present example, the second component of the composite is the same auxetic PE, as mentioned earlier. As follows from Table 3.11, conditions (3.2) and (3.6) hold in a wide η range, however the $(Q_{33}^*)^2$ value is smaller than that predicted for the PMN–0.28PT-based composite, see Table 3.10. This difference between the $(Q_{33}^*)^2$ values of the related composites with auxetic PE is due to the large piezoelectric coefficients $d_{3j}^{(1)}$ of the [001]-poled PMN–0.28PT SC in comparison to $d_{3j}^{(1)}$ of the poled PCR-7M FC, cf. data in Tables 1.3 and 1.5. It should be added for comparison that the g_{33}^* values from Table 3.11 are almost equal to $g_{33}^* = 53 \text{ mV m/N}$ that is related to the aforementioned 1–3-type perforated PZT FC/epoxy composite [57]. The larger $(Q_{33}^*)^2$ values from Table 3.11 in comparison to $(Q_{33}^*)^2$ of 1–3-type perforated PZT FC/epoxy composite [57] are due to the higher piezoelectric activity of the poled PCR-7M FC (see Table 1.5). For instance, the piezoelectric coefficient $d_{33}^{(1)}$ of the PCR-7M FC is approximately two–five times larger than $d_{33}^{(1)}$ of various PZT FC compositions.

Table 3.11 Effective piezoelectric coefficients d_{3j}^* (in pC/N), g_{3j}^* (in mV m/N), and squared figures of merit $(Q_{3j}^*)^2$ (in 10^{-12} Pa^{-1}) of the 1–3-type PCR-7M FC/auxetic PE composite^a at the volume fraction of FC $m = 0.3$

η	d_{31}^*	d_{32}^*	d_{33}^*	g_{31}^*	g_{32}^*	g_{33}^*	$(Q_{31}^*)^2$	$(Q_{32}^*)^2$	$(Q_{33}^*)^2$
0.01	–64.6	47.0	726	–4.78	3.48	53.8	0.309	0.164	39.1
0.1	–44.9	50.9	727	–3.32	3.77	53.8	0.149	0.192	39.1
0.2	–28.7	52.1	728	–2.13	3.86	53.8	0.0611	0.201	39.2
0.4	–5.62	49.7	728	–0.420	3.68	53.8	2.36×10^{-3}	0.183	39.2
0.6	10.5	44.0	729	0.70	3.25	53.9	8.09×10^{-3}	0.143	39.3
0.8	22.0	37.1	729	1.62	2.74	53.9	0.0356	0.102	39.3
1	30.1	30.1	729	2.23	2.23	53.9	0.0671	0.0671	39.3

^aA cross section of the 1–3-type composite is shown in Fig. 2.14. Calculations have been performed by means of FEM

3.7 Hydrostatic Piezoelectric Sensitivity and Figures of Merit

The hydrostatic piezoelectric response of a composite [3, 7] is related to its hydrostatic piezoelectric coefficients d_h^* and g_h^* and squared figure of merit $(Q_h^*)^2$ from (2.1) and (2.2). Important problems for the improvement of the hydrostatic piezoelectric response of poled FCs and piezo-active composites based on FCs were discussed in work [6–8]. The FC and composite materials are used as active elements of hydrophones [3] that are sensitive to hydrostatic pressure, acoustic waves in water etc. A hydrophone sensitivity [3] is associated with a voltage caused by stresses induced by the acoustic pressure, and the larger sensitivity means the larger voltage at the same pressure level. In Sect. 3.7 we consider relations between the piezoelectric coefficients g_{3j}^* and hydrostatic parameters of some SC-based composites.

In a 1–3 PZN–0.07PT SC/PVDF composite, $\max g_{33}^*$ and $\min g_{31}^*$ are observed in Table 3.12 at volume fractions of SC $m \approx 0.05$, i.e., in the volume-fraction region wherein the dielectric permittivity of the composite $\varepsilon_{33}^{*\sigma}$ is small in comparison with $\varepsilon_{33}^{(1),\sigma}$ of its SC component. The m values related to extreme points of g_{3j}^* are larger than those related to extreme points of g_{3j}^* in other piezo-active composites [7, 8, 11, 23, 24] based on either SCs or FCs. This is due to the presence of the second piezoelectric component, i.e., ferroelectric PVDF polymer that strongly influences the PS of the 1–3 composite [26], especially at $m \ll 1$. The value of $\max[(Q_h^*)^2]$ is approximately two–three times larger than $(Q_h^*)^2$ of conventional 1–3 FC/polymer composites [7, 9], and this high performance is achieved not only due to the piezoelectric polymer component but also due to the SC component with a large piezoelectric coefficient $d_{33}^{(1)}$, see Table 1.3.

The important example of the PS and figures of merit is related to the 2–0–2 SC/SC/polymer composite considered in Sect. 3.1. We assume that the Type I layer of the 2–0–2 composite is represented by a [001]-poled SC, and in the Type II layer, spheroidal SC inclusions are regularly distributed in a polymer medium. Hereafter the Type II layer is regarded as a 0–3 SC/polymer composite. A volume-fraction behaviour of the effective parameters of the 2–0–2 composite based on the [001]-poled KNNTL:Mn SC is shown in Fig. 3.11. We remind that some characteristics of this composite were also highlighted in Fig. 3.2. In the presence of the Type II layer with the system of the aligned highly oblate SC inclusions ($\rho_i \gg 1$), we achieve the considerable hydrostatic PS and figure of merit. The graphs in Fig. 3.11a–c suggest that on increasing the volume fraction m_i of the SC inclusions in the Type II layer, the piezoelectric coefficients $|g_{3j}^*|$ decrease at $m = \text{const}$. However the decrease of the piezoelectric coefficient g_{33}^* is less pronounced (Fig. 3.11c) in comparison to $|g_{31}^*|$ (Fig. 3.11a) and $|g_{32}^*|$ (Fig. 3.11b), i.e., the transverse PS of the composite decreases more rapidly than its longitudinal PS. Such a feature of the piezoelectric performance of the studied 2–0–2 composite

Table 3.12 Effective piezoelectric coefficients d_{3j}^* (in pC/N), g_{3j}^* (in mV/mN), and squared figures of merit $(Q_{33}^*)^2$ and $(Q_h^*)^2$ (in 10^{-12} Pa $^{-1}$) which have been calculated for the 1–3 [001]-poled PZN–0.07PT SC/PVDF composite^a by using the FEM and matrix method^b

m	$-d_{31}^*$	d_{33}^*	$-g_{31}^*$	g_{33}^*	$(Q_{33}^*)^2$	$(Q_h^*)^2$
0.01	5.02 (5.08)	18.4 (18.3)	34.6 (35.3)	127 (127)	2.34 (2.32)	0.482 (0.460)
0.03	35.8 (36.0)	119 (119)	106 (107)	353 (353)	42.0 (42.0)	6.68 (6.53)
0.05	66.1 (66.5)	216 (215)	110 (111)	361 (360)	78.0 (77.4)	11.8 (11.3)
0.07	96.1 (96.6)	308 (307)	105 (105)	335 (334)	103 (103)	14.5 (14.1)
0.09	126 (126)	396 (396)	96.7 (96.7)	304 (304)	120 (120)	15.9 (15.9)
0.12	170 (170)	522 (522)	86.0 (86.0)	264 (264)	138 (138)	16.7 (16.7)
0.20	283 (283)	823 (823)	65.7 (65.7)	191 (191)	157 (157)	15.3 (15.3)
0.30	418 (418)	1140 (1140)	51.7 (51.7)	141 (141)	161 (161)	11.4 (11.4)
0.40	546 (545)	1410 (1410)	43.0 (43.3)	111 (112)	157 (158)	8.12 (8.28)
0.50	668 (667)	1650 (1650)	37.3 (37.2)	92.1 (92.1)	152 (152)	5.36 (5.49)
0.60	785 (784)	1850 (1850)	33.3 (33.2)	78.4 (78.4)	145 (145)	3.31 (3.40)
0.70	896 (895)	2030 (2030)	30.1 (30.1)	68.3 (68.3)	139 (139)	1.86 (1.91)
0.80	1000 (1000)	2190 (2190)	27.6 (27.6)	60.5 (60.5)	132 (132)	0.901 (0.914)
0.90	1110 (1110)	2330 (2330)	25.9 (25.9)	54.3 (54.3)	127 (127)	0.320 (0.322)
0.99	1200 (1200)	2440 (2440)	24.4 (24.4)	49.7 (49.7)	121 (121)	0.0600 (0.0599)

^aSee the schematic of the composite in Fig. 2.11. The spontaneous polarisation of the SC component is $P_s^{(1)} \uparrow \uparrow OX_3$, and the remanent polarisation of the polymer component is $P_r^{(2)} \uparrow \uparrow OX_3$
^bValues of the effective parameters calculated using the matrix method are given in parentheses

leads to large values of $(Q_h^*)^2$ (Fig. 3.11b) in wide ranges of volume fractions m and m_i . The non-monotonic behaviour of $(Q_h^*)^2$ at $m = \text{const}$ (Fig. 3.11d) is caused by the elastic anisotropy of the Type II layer to a large extent. We underline that, despite the smaller piezoelectric coefficient $d_{33}^{(1)}$ of the KNNTL:Mn SC [48] in comparison with $d_{33}^{(1)}$ of the PZN–0.07PT SC, the value of $\max[(Q_h^*)^2]$ shown in Fig. 3.11d is about two times larger than that related to the PZN–0.07PT-based

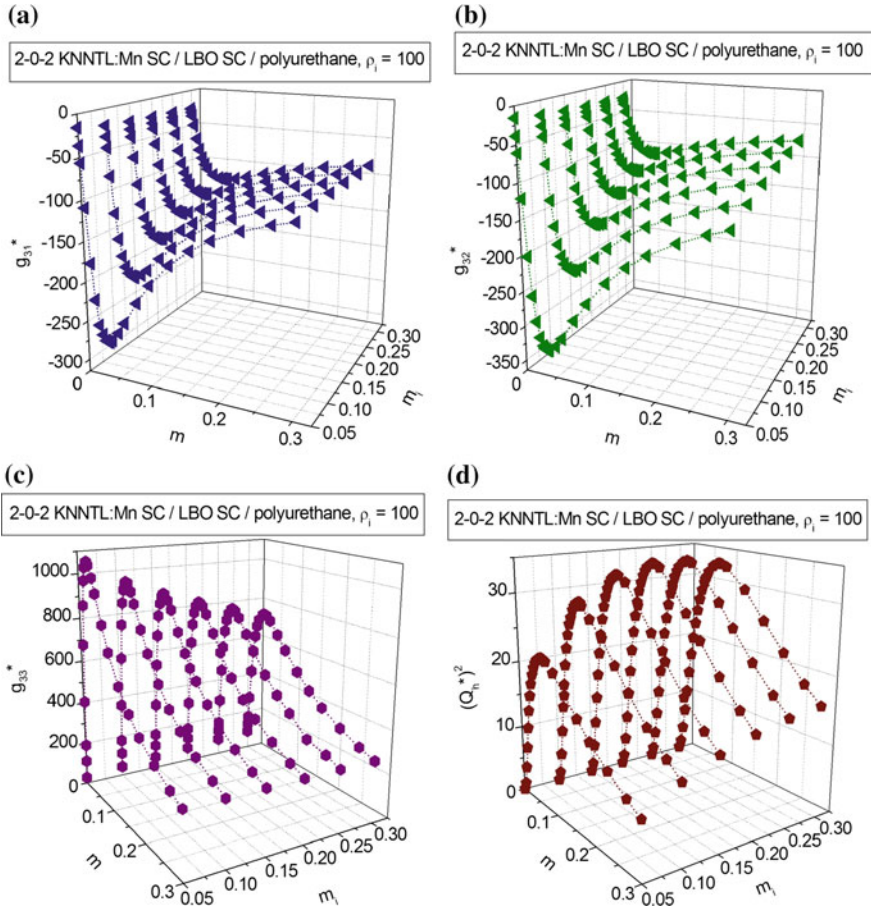


Fig. 3.11 Volume-fraction dependences of piezoelectric coefficients g_{3j}^* (a–c, in mV m/N) and hydrostatic squared figure of merit $(Q_h^*)^2$ (d, in 10^{-12} Pa^{-1}) of the 2–0–2 [001]-poled KNNTL:Mn SC/LBO SC/polyurethane composite

composite, see Table 3.12. This is mainly achieved due to the large piezoelectric coefficient $g_{33}^{(1)} = 94.7 \text{ mV m/N}$ of the KNNTL:Mn SC [48].

In Table 3.13 we show changes in the PS and squared figures of merit of the same 2–0–2 composite based on the KNNTL:Mn SC at variations of the microgeometric characteristics of the Type II layer and the volume fraction m of SC in the Type I layer. Changes in the aspect ratio ρ_i and volume fraction m_i of the SC inclusions in the Type II layer are to be taken into account at the prediction of the longitudinal PS and hydrostatic response: these changes strongly influence the elastic anisotropy of the Type II layer and, therefore, weaken the transverse PS of the composite as a whole. Due to this weakening at $\rho_i \gg 1$, we observe large $(Q_h^*)^2$ values (Table 3.13) that undergo minor changes at volume fraction $m = \text{const}$

Table 3.13 Effective piezoelectric coefficients g_{33}^* and g_h^* (in mV m/N), and squared figures of merit $(Q_{33}^*)^2$ and $(Q_h^*)^2$ (in 10^{-12} Pa $^{-1}$) of the 2–0–2 [001]-poled KNNTL:Mn SC/LBO SC/polyurethane composite^a

ρ_i	m_i	m	g_{33}^*	g_h^*	$(Q_{33}^*)^2$	$(Q_h^*)^2$
0.01	0.10	0.05	745	162	59.1	2.78
		0.10	594	121	81.0	3.34
		0.15	470	90.8	87.3	3.26
		0.20	385	70.9	87.9	2.98
		0.25	324	56.9	86.4	2.66
		0.30	280	46.7	83.9	2.33
1	0.10	0.05	1000	214	121	5.55
		0.10	715	141	146	5.69
		0.15	534	99.3	141	4.89
		0.20	422	74.3	131	4.07
		0.25	348	58.1	121	3.37
		0.30	296	46.7	112	2.80
100	0.10	0.05	931	98	94.2	26.9
		0.10	688	335	119	28.1
		0.15	521	231	119	23.3
		0.20	415	168	113	18.5
		0.25	344	127	106	14.5
		0.30	293	99.2	99.6	11.4
0.01	0.20	0.05	569	135	33.6	1.89
		0.10	491	105	48.9	2.26
		0.15	409	82.8	56.4	2.31
		0.20	346	66.5	60.1	2.22
		0.25	299	54.6	61.9	2.06
		0.30	262	45.4	62.7	1.88
1	0.20	0.05	876	197	89.2	4.51
		0.10	666	135	117	4.78
		0.15	511	96.2	119	4.21
		0.20	409	72.4	114	3.58
		0.25	340	56.8	108	3.01
		0.30	291	45.8	102	2.52
100	0.20	0.05	829	529	71.8	29.3
		0.10	646	380	96.5	33.4
		0.15	500	270	99.5	29.0
		0.20	403	199	96.7	23.6
		0.25	336	152	92.4	18.8
		0.30	288	118	87.8	14.8

^aThe EFM and matrix method were applied to evaluate the electromechanical properties of the 0–3 SC/polymer layer and 2–0–2 SC/SC/polymer composite, respectively

(Type I layer) and on increasing the volume fraction m_i of SC in the Type II layer. The dielectric properties of the Type II layer influence the PS, $(Q_{33}^*)^2$ and $(Q_h^*)^2$ of the composite to a restricted degree only. It should be added that the large g_{33}^* and $(Q_h^*)^2$ values of the studied lead-free 2–0–2 composite (see data in Fig. 3.11c, d and Table 3.13) are important in piezoelectric sensor, hydroacoustic and other applications.

3.8 Conclusion

This chapter has been devoted to the piezoelectric coefficients g_{ij}^* , their anisotropy and links between microgeometric characteristics of piezo-active composites and their PS. As follows from numerous papers, experimental and theoretical studies on the composites, their piezoelectric coefficients g_{ij}^* play an important role for the description of the PS, figures of merit and related characteristics. Specific trends in improving the PS of the composite and increasing its piezoelectric coefficients g_{ij}^* have been discussed for specific connectivity patterns. The main results of this chapter are formulated as follows.

- (i) Examples of the PS concerned with the piezoelectric coefficients g_{ij}^* and related parameters of are discussed for the 0–3-type, 1–1-type, 1–3-type, 2–2-type, and 3– β composites. The studied composites are based on either FCs or domain-engineered SCs, and examples of the composite patterns with planar and non-planar interfaces are analysed.
- (ii) Various volume-fraction dependences of the piezoelectric coefficients g_{ij}^* of the studied two- and three-component composites are characterised by relatively sharp extreme of g_{3j}^* at small volume fractions m of the main piezoelectric component that is represented by FC, ferroelectric SC etc. Along with the drastic changes in g_{3j}^* , examples of the ‘sleeping PS’ are observed. This feature of the studied piezo-active composites is caused by the strong influence of the dielectric properties and system of interfaces on g_{3j}^* . Elastic properties of the composite influence the PS of the composites to a lesser degree. An additional opportunity to change the piezoelectric coefficients g_{3j}^* is concerned with the elastic anisotropy that can be large in porous and heterogeneous polymer matrices or layers. In contrast to g_{3j}^* , the shear piezoelectric coefficients (e.g. g_{15}^* or g_{24}^*) undergo less considerable changes in the wide volume-fraction range, and such a behaviour is associated with some microgeometric features of the composites.
- (iii) Because of the small volume fractions m at which extreme of the piezoelectric coefficients g_{3j}^* and g_h^* are achieved in the studied composites, values of $m < 0.1$ are to be chosen on manufacturing. In this case, one can keep the high PS and avoid a significant decrease of $\max|g_{3j}^*|$ and $\max g_h^*$.
- (iv) The auxetic polymer component influences the PS and anisotropy of the piezoelectric coefficients g_{3j}^* , especially at volume fractions of the main piezoelectric component $m \ll 1$. A use of the auxetic polymer component enables one to reach a change in sign of some piezoelectric coefficients g_{3j}^* of the studied composites and becomes a good stimulus to form highly anisotropic composite structures.
- (v) As follows from the performance of the lead-free composites based on the domain-engineered KNNTL:Mn SC, the high PS and large values of squared figures of merit of the composites are mainly achieved due to the large

piezoelectric coefficient $g_{33}^{(1)}$ of their SC component. The high PS of the studied lead-free composites can be regarded as their advantage over the conventional FC/polymer composites.

- (vi) The present results show the potential of the studied composites that are suitable for piezoelectric sensor, transducer, energy-harvesting, and hydroacoustic applications.

References

1. Zheludev IS (1971) *Physics of crystalline dielectrics. Vol 2: Electrical properties.* Plenum, New York
2. Steinem C, Janshoff A (eds) (2007) *Piezoelectric sensors.* Springer, Berlin
3. Sherman CH, Butler JL (2007) *Transducers and arrays for underwater sound.* Springer, New York
4. Fraden J (2010) *Handbook of modern sensors. Physics, designs, and applications.* Springer, New York
5. Sharapov V (2011) *Piezoceramic sensors.* Springer, Heidelberg
6. Lupeiko TG, Lopatin SS (2004) Old and new problems in piezoelectric materials research and materials with high hydrostatic sensitivity. *Inorg Mater* 40 (Suppl. 1):S19–S32
7. Topolov VYu, Bowen CR (2009) *Electromechanical properties in composites based on ferroelectrics.* Springer, London
8. Topolov VYu, Bisegna P, Bowen CR (2014) *Piezo-active composites. Orientation effects and anisotropy factors.* Springer, Berlin
9. Akdogan EK, Allahverdi M, Safari A (2005) Piezoelectric composites for sensor and actuator applications. *IEEE Trans Ultrason Ferroelectr Freq Control* 52:746–775
10. Zhang S, Li F (2012) High performance ferroelectric relaxor-PbTiO₃ single crystals: status and perspective. *J Appl Phys* 111:031301
11. Topolov VYu, Krivoruchko AV, Bowen CR (2012) Anisotropy of electromechanical properties and hydrostatic response of advanced 2–2-type composites. *Physica Status Solidi A* 209:1334–1342
12. Topolov VYu, Glushanin SV (2009) Features of the hydrostatic piezoelectric response of a novel 2–2–0 composite based on single-domain 0.67Pb(Mg_{1/3}Nb_{2/3})O₃–0.33PbTiO₃ crystal. *Compos Sci Technol* 69:2532–2537
13. Topolov VYu, Bowen CR, Ermakov IA (2016) Remarkable hydrostatic piezoelectric response of novel 2–0–2 composites. *Ferroelectr Lett Sect* 43:90–95
14. Grekov AA, Kramarov SO, Kuprienko AA (1987) Anomalous behavior of the two-phase lamellar piezoelectric texture. *Ferroelectrics* 76:43–48
15. Adachi M, Shiosaki T, Kobayashi H, Ohnishi O, Kawabata A (1985) Temperature compensated piezoelectric lithium tetraborate crystal for high frequency surface acoustic wave and bulk wave device applications. In: *Proceedings of 1985 IEEE Ultrasonics Symposium, IEEE, New York*, pp 228–232
16. Ikegami S, Ueda I, Nagata T (1971) Electromechanical properties of PbTiO₃ ceramics containing La and Mn. *J Acoust Soc Am* 50:1060–1066
17. Nagatsuma K, Ito Y, Jyomura S, Takeuchi H, Ashida S (1985) Elastic properties of modified PbTiO₃ ceramics with zero temperature coefficients. In: Taylor GW (ed) *Ferroelectricity and related phenomena. Piezoelectricity, vol 4.* Gordon and Breach Science Publishers, New York, pp 167–176

18. Gusakova LG, Poguibko VM, Spiridonov NA, Ishchuk VM, Kisel NK (2012) Lead-free nanostructured piezoceramic material based on (K, Na)NbO₃. *Nanosyst Nanomater Nanotechnol* 10:303–312 (in Russian)
19. Yan Y, Zhou JE, Maurya D, Wang YU, Priya S (2016) Giant piezoelectric voltage coefficient in grain-oriented modified PbTiO₃ material. *Nat Commun* 7:13089
20. Topolov VYu, Krivoruchko AV (2009) Polarization orientation effect and combination of electromechanical properties in advanced 0.67Pb(Mg_{1/3}Nb_{2/3})O₃–0.33PbTiO₃ single crystal/polymer composites with 2–2 connectivity. *Smart Mater Struct* 18:065011
21. Grekov AA, Kramarov SO, Kuprienko AA (1989) Effective properties of a transversely isotropic piezoelectric composite with cylindrical inclusions. *Mech Compos Mater* 25:54–61
22. Chan HLW, Unsworth J (1989) Simple model for piezoelectric ceramic/polymer 1–3 composites used in ultrasonic transducer applications. *IEEE Trans Ultrason Ferroelectr Freq Control* 36:434–441
23. Gibiansky LV, Torquato S (1997) On the use of homogenization theory to design optimal piezocomposites for hydrophone applications. *J Mech Phys Solids* 45:689–708
24. Bezus SV, Topolov VYu, Bowen CR (2006) High-performance 1–3-type composites based on (1 – x) Pb(A_{1/3}Nb_{2/3})O₃–xPbTiO₃ single crystals (A = Mg, Zn). *J Phys D Appl Phys* 39:1919–1925
25. Wang F, He C, Tang Y (2007) Single crystal 0.7Pb(Mg_{1/3}Nb_{2/3})O₃–0.3PbTiO₃/epoxy 1–3 piezoelectric composites prepared by the lamination technique. *Mater Chem Phys* 105:273–277
26. Topolov VYu, Krivoruchko AV, Bisegna P, Bowen CR (2008) Orientation effects in 1–3 composites based on 0.93Pb(Zn_{1/3}Nb_{2/3})O₃–0.07PbTiO₃ single crystals. *Ferroelectrics* 376:140–152
27. Topolov VYu, Bisegna P (2010) Anisotropic piezoelectric properties of 1–3 ceramic/polymer composites comprising rods with elliptic cross section. *J Electroceram* 25:26–37
28. Topolov VYu, Bowen CR, Bisegna P, Krivoruchko AV (2015) New orientation effect in piezo-active 1–3-type composites. *Mater Chem Phys* 151:187–195
29. Bowen CR, Topolov VYu, Isaeva AN, Bisegna P (2016) Advanced composites based on relaxor-ferroelectric single crystals: from electromechanical coupling to energy-harvesting applications. *CrystEngComm* 18:5986–6001
30. Topolov VYu, Bowen CR, Bisegna P (2015) New aspect-ratio effect in three-component composites for piezoelectric sensor, hydrophone and energy-harvesting applications. *Sens Actuators A – Phys* 229:94–103
31. Topolov VYu, Bowen CR, Bisegna P, Panich AE (2015) Effect of the matrix subsystem on hydrostatic parameters of a novel 1–3-type piezo-composite. *Funct Mater Lett* 8:1550049
32. Topolov VYu, Krivoruchko AV, Bisegna P (2011) Electrochemical coupling and its anisotropy in a novel 1–3–0 composite based on single-domain 0.58Pb(Mg_{1/3}Nb_{2/3})O₃–0.42PbTiO₃ crystal. *Compos Sci Technol* 71:1082–1088
33. Glushanin SV, Topolov VYu (2001) Features of electromechanical properties of piezoelectric composites with elements of connectivity 1–1. *J Phys D Appl Phys* 34:2518–2529
34. Glushanin SV, Topolov VYu (2001) Anisotropy of the electromechanical properties and a high piezoelectric sensitivity of the 1–1 type ferroelectric piezocomposites. *Tech Phys Lett* 27:626–628
35. Chan HLW, Ng PKL, Choy CL (1999) Effect of poling procedure on the properties of lead zirconate titanate/vinylidene fluoride-trifluoroethylene composites. *Appl Phys Lett* 74:3029–3031
36. Ng KL, Chan HLW, Choy CL (2000) Piezoelectric and pyroelectric properties of PZT/P(VDF-TrFE) composites with constituent phases poled in parallel or antiparallel directions. *IEEE Trans Ultrason Ferroelectr Freq Control* 47:1308–1315
37. Venkatragavaraj E, Satish B, Vinod PR, Vijaya MS (2001) Piezoelectric properties of ferroelectric PZT–polymer composites. *J Phys D Appl Phys* 34:487–492
38. Chiang CK, Popielarz R (2002) Polymer composites with high dielectric constant. *Ferroelectrics* 275:1–9

39. Wilson SA, Maistros GM, Whatmore RW (2005) Structure modification of 0–3 piezoelectric ceramic/polymer composites through dielectrophoresis. *J Phys D Appl Phys* 38:175–182
40. Glushanin SV, Topolov VYu, Krivoruchko AV (2006) Features of piezoelectric properties of 0–3 PbTiO₃-type ceramic/polymer composites. *Mater Chem Phys* 97:357–364
41. Topolov VYu, Turik AV, Chernobabov AI (1994) On the mechanism of high piezoelectric anisotropy in lead titanate-based ferroelectrics. *Crystallogr Rep* 39:805–809
42. Topolov VYu, Turik AV, Chernobabov AI (1994) On the piezoelectric anisotropy in modified PbTiO₃ ceramics. *Ferroelectrics* 154:271–276
43. Ngoma JB, Cavaille JY, Paletto J, Perez J (1990) Dielectric and piezoelectric properties of copolymer-ferroelectric composite. *Ferroelectrics* 109:205–210
44. Gururaja TR, Safari A, Newnham RE, Cross LE (1988) Piezoelectric ceramic-polymer composites for transducer applications. In: Levinson M (ed) *Electronic ceramics: properties, devices, and applications*. Marcel Dekker, New York, pp 92–128
45. Lushcheykin GA (1987) Polymer and composition piezoelectrics. *Izvestiya Akademii Nauk SSSR Seriya Fizicheskaya* 51:2273–2276 (in Russian)
46. Pardo L, Mendiola J, Alemany C (1988) Theoretical treatment of ferroelectric composites using Monte Carlo calculations. *J Appl Phys* 64:5092–5097
47. Babu I, van den Ende DA, de With G (2010) Processing and characterization of piezoelectric 0–3 PZT/LCT/PA composites. *J Phys D Appl Phys* 43:425402
48. Huo X, Zhang R, Zheng L, Zhang S, Wang R, Wang J, Sang S, Yang B, Cao W (2015) (K, Na, Li)(Nb, Ta)O₃:Mn lead-free single crystal with high piezoelectric properties. *J Am Ceram Soc* 98:1829–1835
49. Kar-Gupta R, Venkatesh TA (2007) Electromechanical response of 1–3 piezoelectric composites: an analytical model. *Acta Mater* 55:1093–1108
50. Sessler GM (1981) Piezoelectricity in polyvinylidene fluoride. *J Acoust Soc Am* 70:1596–1608
51. Topolov VYu, Bisegna P, Glushanin SV, Panich AA (2011) Interrelations between microstructure and piezoelectric sensitivity in novel 0–3–0 composites based on 0.67Pb(Mg_{1/3}Nb_{2/3})O₃–0.33PbTiO₃ single crystal. *Ferroelectrics* 413:11–28
52. Topolov VYu, Bisegna P, Bowen CR (2011) Analysis of the piezoelectric performance of modern 0–3-type composites based on relaxor-ferroelectric single crystals. *Ferroelectrics* 413:176–191
53. Cheng X, Huang S, Chang J, Lu L, Liu F, Ye Z, Wang S (2005) Dielectric and piezoelectric properties of piezoelectric ceramic–sulphoaluminate cement composites. *Smart Mater Struct* 14:N59–N63
54. Smay JE, Tuttle B, Cesarano J III (2008) Robocasting of three-dimensional piezoelectric structures. In: Safari A, Akdoğan EK (eds) *Piezoelectric and acoustic materials for transducer applications*. Springer, New York, pp 305–318
55. Smay JE, Cesarano J III, Tuttle BA, Lewis JA (2002) Piezoelectric properties of 3–X periodic Pb(Zr_xTi_{1-x})O₃–polymer composites. *J Appl Phys* 92:6119–6127
56. Filippov SE, Vorontsov AA, Topolov VYu, Brill OE, Bisegna P, Panich AE (2014) Features of the piezoelectric effect in a novel PZT-type ceramic/clay composite. *Ferroelectr Lett Sect* 41:82–88
57. Mendiola J, Jimenez B (1984) Review of recent work on piezoelectric composite systems. *Ferroelectrics* 53:159–166
58. Bowen CR, Topolov VYu, Kim HA (2016) *Modern piezoelectric energy-harvesting materials*. Springer International Publishing, Switzerland